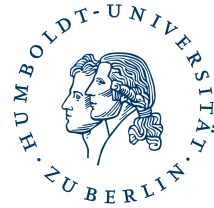


Humboldt-Universität zu Berlin  
Institut für Physik  
Newtonstrasse 15, 12489 Berlin



# HIGH ORDER HARMONIC GENERATION AS A POSSIBLE SEED SOURCE FOR THE BESSY FREE ELECTRON LASER

Diplomarbeit

Torsten Leitner

geb. am 16.09.1979 in Rotthalmünster

Matrikelnummer: 197597

vorgelegt am: 13. August 2007

1. Gutachter: Prof. Dr. Eberhard Jaeschke
2. Gutachter: PD Dr. Alejandro Saenz



## Kurzzusammenfassung

Die *Berliner Elektronenspeicherring-Gesellschaft für Synchrotronstrahlung* (BESSY) plant den Bau eines *Freie Elektronen Lasers* (FEL) [1], der auf dem Prinzip der *High-Gain Harmonic Generation* (HGHG) [2] basiert. In einem HGHG-FEL wird der Lichtentstehungsprozess durch ein externes elektromagnetisches Feld initiiert, den *Seed*. Die BESSY *Soft X-ray FEL-Anlage* wird drei FEL-Linien beinhalten, von denen jede aus einer Kaskade von mehreren HGHG-Stufen besteht. Die einzelnen HGHG-Stufen werden aus einem Undulator, einer magnetischen Verzögerungseinheit und einem weiteren Undulator aufgebaut. Als Seed-Quelle für die drei FEL-Linien sollen durchstimmbare Laser dienen, deren Wellenlängen in einem Bereich von 230 nm bis 460 nm variiert werden können. Durchlaufen das Seed-Feld und der Elektronenstrahl gemeinsam eine HGHG-Stufe, so wird ein neues Seed-Feld erzeugt, dessen Frequenz ein Vielfaches der Frequenz des ursprünglichen elektromagnetischen Feldes beträgt. Dieser Prozess wird so lange fortgesetzt, bis die erwünschte Wellenlänge von einigen wenigen Nanometer erreicht ist. Ein direktes *Seeding* in, oder nahe am Zielwellenlängenbereich wird angestrebt. Dadurch lässt sich die Aufheizung des Elektronenstrahls beim Durchlauf durch die Undulatoren signifikant verringern und die Verstärkung von Rauscheffekten während der Frequenzumwandlung vermeiden [3]. Dies führt zu einer besseren Qualität der FEL Ausgangsstrahlung [1].

*High-order Harmonic Generation* (HHG) in einem Gasmedium ist eine geeignete Methode um solch kurze Wellenlängen im nanometer Bereich zu erzeugen. Bestrahlt man ein Gas mit einem hochintensiven Laser, so werden einige Atome ionisiert. Bei der anschließenden Rekombination strahlen die Atome kohärentes Licht bei einem geradzahigen Vielfachen der Frequenz des erregenden Lasers ab. Im Rahmen dieser Arbeit wurde ein Programm entwickelt, das die Entstehung der Lichtspektren einzelner Atome gemäß der *Strong-Field Approximation* (SFA) [4] simuliert und die kollektive Evolution des makroskopischen Lichtfelds aller Atome im Gasmedium mithilfe einer radial-symmetrischen Diffusionsgleichung berechnet. Das Ergebnis der HHG-Simulation wird als Seed an GENESIS 1.3 [5], einem FEL-Simulationsprogramm, übergeben, um den FEL-Prozess mit HHG Seed zu untersuchen.



## Abstract

The *Berliner Elektronenspeicherring-Gesellschaft für Synchrotronstrahlung* (BESSY) plans to build a free electron laser (FEL) [1], based on the *High-Gain Harmonic Generation* (HGHG) principle [2]. In this concept, the FEL process is initiated by an external light field, the *seed*. It is planned to use tunable lasers as seeding sources with wavelengths ranging from 230 nm to 460 nm. The seeding radiation and the electron beam pass through several HGHG stages, each consisting of an undulator – magnetic delay – undulator unit, where the light frequency is upconverted to a higher harmonic. This process will be repeated until the desired wavelength of a few nanometer is achieved. Seeding directly at shorter wavelengths close to or in the final output range is desirable as the noise amplification during the frequency upconversion can be avoided [3]. In addition, heating effects occurring while the electron beam passes through the cascades are significantly reduced. This improves the quality of the FEL output radiation [1].

To produce these short wavelengths *High-order Harmonic Generation* (HHG) in gases is a promising tool. If a gas is irradiated by a high intensity laser, some atoms are ionized. Upon recombination, the atoms coherently radiate at odd integer multiples of the fundamental laser frequency. For this purpose a numerical simulation based on the *Strong-Field Approximation* (SFA) [4] was developed, which calculates the single atom spectra and the propagation of the produced light through the gas. Using this radiation as the seed, the FEL process is analyzed via GENESIS 1.3 simulations [5].



---

# Contents

---

<b>1</b>	<b>Introduction</b>	<b>3</b>
<b>2</b>	<b>High Order Harmonic Generation</b>	<b>7</b>
2.1	Simple Man Model . . . . .	7
2.2	Strong Field Approximation . . . . .	14
2.3	Propagation in the Medium . . . . .	18
<b>3</b>	<b>HHG Simulation</b>	<b>21</b>
3.1	Assumptions and Numerical Methods . . . . .	21
3.2	Single Atom Spectra . . . . .	23
3.3	Propagation . . . . .	24
3.3.1	Solving the Propagation Equation . . . . .	24
3.3.2	Stability Analysis . . . . .	26
3.4	Simulation Sequence . . . . .	28
<b>4</b>	<b>HHG Simulation Results</b>	<b>33</b>
4.1	Cut-off Law . . . . .	33
4.2	Influence of the Laser Pulse Length . . . . .	35
4.3	Phase Matching . . . . .	35
<b>5</b>	<b>FEL Simulations with Genesis 1.3</b>	<b>41</b>
5.1	The HHG Seed . . . . .	41
5.2	STARS . . . . .	43
5.3	HHG Seeding of the BESSY Low-Energy FEL . . . . .	50
<b>6</b>	<b>Conclusion</b>	<b>53</b>
<b>A</b>	<b>Solution of the Schrödinger Equation</b>	<b>i</b>
<b>B</b>	<b>Stationary Phase Approximation</b>	<b>v</b>
<b>C</b>	<b>Stability Analysis of the Propagation Routine</b>	<b>ix</b>
<b>D</b>	<b>Additional HHG Spectra</b>	<b>xi</b>
	<b>Bibliography</b>	<b>xiii</b>
	<b>Acknowledgement</b>	<b>xv</b>

## CONTENTS

---

---

# 1

## Introduction

---

Nanotechnological applications are already state-of-the-art in many sectors of our daily life. During the last decades, the scales for the applied sciences have shifted more and more to the nano, pico and even femto ranges. Therefore the community of scientists is demanding for new light sources providing higher photon energies to achieve wavelengths in the few nanometer or even ångström regime together with high brilliance and coherence. The number of envisaged experiments is large and includes femtochemistry, high resolution imaging, investigation of molecular and atomic dynamics and many further applications [6]. The Free Electron Laser (FEL) can meet all these requirements. It provides full transverse coherent light at sufficiently small wavelengths.

In a FEL, an accelerated electron beam is passed through an undulator, whose alternating magnetic fields forces the electrons on a sinusoidal wiggling trajectory. Therefore the electrons can couple to an external light field or to their own spontaneously emitted synchrotron radiation. The FEL resonant wavelength is determined by the energy of the electron beam and the properties of the undulator section. Due to the lack of suitable mirrors, short wavelengths, i.e. in the nanometer range, can only be achieved by single pass FELs [1]. There are two basic concepts of single pass FELs: *Self Amplified Spontaneous Emission* (SASE) and seeded *High Gain Harmonic Generation* (HGFG) [2]. Both were proposed and built all over the world in the past years [1, 7, 8, 9, 10].

The SASE FEL process starts from the spontaneous emission of the electron beam, which is then amplified due to the interaction between the electrons and the radiation inside the undulator. This scheme lacks full control of the duration of the generated X-ray pulse. As it starts from shot noise, the output power and spectra are stochastic [11].

The second concept, the HGFG FEL, uses a laser beam as a seed copropagating with the electrons in a first undulator. In this so-called *modulator*, which is tuned resonant to the frequency of the fundamental laser, the electrons couple to the external electro-magnetic field such that an energy modulation occurs. By means of a dispersive section, this energy modulation is then converted into a spatial modulation or *bunching*, which is optimized to a particular harmonic. After that, the prebunched electron beam is inserted into a second undulator, the *radiator*. To reach the few nm to sub-nm scale, cascades of HGFG stages are used, where each stage seeds the next and is tuned to radiate at a multiple frequency of the previous stage, so that in each unit the light field is converted to a higher harmonic order until the desired output is achieved.

Direct seeding at shorter wavelengths would simplify and shorten the FEL setup, but due to the lack of suitable conventional lasers, the cascading HGHG scheme appeared to be the only way to provide high power seeds in the nanometer range. However, in modern optics *High-order Harmonic Generation* (HHG) is a new, rapidly rising field of interest. It offers the possibility of generating a train of attosecond pulses consisting of a superposition of many odd multiples of the fundamental laser frequency. The whole pulse train can be supplied directly as a seed to a HGHG FEL, whose resonant wavelength is tuned to the desired harmonic. As the FEL process itself is highly frequency selective [12, 13, 14], only the resonant harmonic will be amplified in the FEL radiator, thus no spectral filters have to be applied to the HHG signal.

To produce such higher harmonics down to (sub-)nm wavelengths, a very strong laser field with an intensity in the range of  $10^{14}$  to  $10^{15}$   $W/cm^2$  has to be applied to a gas target. In a semiclassical view, HHG can be described as a three step process. The laser first bends the coulombic potential of the atomic core, in which the electron is trapped, thus creating a coulombic wall. This results in a finite quantum mechanical probability for the electron to escape the atom by tunneling through the potential wall. When the electron appears in the continuum, it is immediately accelerated away from the core by the strong electric field of the laser. After the electric field changes its sign, the electron is strongly driven back to the atom and radiative recombination of the electron and the ionic core can occur with a certain probability. The highest frequencies that can be reached are linked to the depth of the core potential, given by the ionization potential  $I_p$ , and to the strength of the laser described by the ponderomotive potential of a free electron in a laser field  $U_p$ . This semiclassical view, as well as a more detailed quantum mechanical calculation result in an experimentally confirmed, simple *cut-off* law for the maximum frequency  $\omega_c$  to be found in the harmonic spectra:  $\omega_c \sim I_p + 3.17 U_p$ .

Evidently, planning, designing and building large user facilities like seeded FELs require a deep insight into the participating physical phenomena. Therefore simulations are mandatory wherever closed analytic expressions are not available. To allow a numerical investigation of the new approach of high harmonic seeded FELs, the main goal of this work was to develop a simulation code based on the *Strong Field Approximation* (SFA) [4]. The code calculates the high harmonic spectra produced inside a gas filled cell including effects on the fundamental laser and the harmonics due to the propagation inside the medium. Using this radiation as a seed, the FEL process can be further analyzed via a numerical simulation with the 3D FEL code GENESIS 1.3 [5].

The *Simple Man Model* of HHG is described in section 2.1 of this work. Some of the major aspects are derived from this simple, semiclassical view. In section 2.2, the SFA is introduced. It is a fully quantum mechanical approach on

---

HHG which approximately solves the corresponding time-dependent Schrödinger equation (TDSE) within the tunneling ionization regime of parameters. The evolution of the fundamental laser beam and the generated HHG light inside the gas medium are discussed in section 2.3. Chapter 3 addresses the simulation of the HHG process in a gas medium. The program sequence and numerical problems while implementing the code will be discussed. In the chapters 4 and 5 results for selected HHG and seeded FEL simulations will be presented. The main part of this thesis ends with a conclusion given in chapter 6. In an appendix, closer views on some mathematical derivations are given, which did not fit into the main document and additional HHG simulation results are depicted. A bibliography and the acknowledgement can be found at the very end of this report.



---

## 2

# High Order Harmonic Generation

---

High-order harmonic generation occurs when an intense laser field interacts with an atomic gas target. When rare gas atoms are irradiated by sub-100-fs pulses with peak powers of the order of  $10^{13}$  to  $10^{15}$   $W/cm^2$ , the gas medium responds in a highly non-linear way, generating radiation with higher frequencies copropagating with the fundamental laser beam. In general, the obtained spectra consist of the fundamental frequency  $\omega_0$  plus its odd multiples  $\omega_q = q\omega_0$ ,  $q \in (2N + 1)$  up to the cut-off frequency, where the spectrum ends abruptly. .

In the first section of this chapter a simplified semiclassical model to allow for a understanding of the major aspects on HHG is presented.

The chapter continues with a quantummechanical approach that describes the HHG process for a single atom in terms of a time dependent Schrödinger equation (in atomic units):

$$i\frac{d}{dt}|\Psi(\vec{r}, t)\rangle = \left[ -\frac{1}{2}\hat{\nabla}^2 + \hat{V}(\mathbf{x}) - E(t) \hat{x} \right] |\Psi(\vec{r}, t)\rangle . \quad (2.1)$$

As there is no closed analytical solution and as a full simulation of this equation would result in a rather time consuming application, an approximate, widely used, solution of eq.(2.1) is introduced in section 2.2.

The last section of this chapter presents a set of equations to allow for the evolution of the harmonic light and the laser beam through an irradiated gas medium.

## 2.1 Simple Man Model

The *Simple Man Model* represents a semiclassical view on the HHG process which reproduces some of the major aspects of the experimental results on HHG and provides a clear understanding. This model is only valid in the so called tunneling regime, where the fundamental laser frequency  $\omega_0$  is characterized by:

$$\hbar\omega_0 \ll I_p \ll U_p , \quad (2.2)$$

with the ionization potential of the atom  $I_p$  and the ponderomotive potential  $U_p = e^2 E^2 / (4m\omega_0^2)$  of an electron in the electric field of the laser.

The Simple Man Model describes high-order harmonic generation as a three-step process, see figure 2.1.

1. An atom is ionized by a strong laser field producing a parent ion and a free electron with no kinetic energy at a time  $t_i$
2. The electron is immediately accelerated by the laser electric field. When the field changes its sign, the electron is driven back to the atomic core.
3. If the electron and the parent ion collide and recombine at a time  $t_f$ , the gained kinetic energy  $E_{kin}$  of the electron plus the binding energy is emitted via a photon of the frequency  $\omega_q = (E_{kin} + I_p)/\hbar$ .

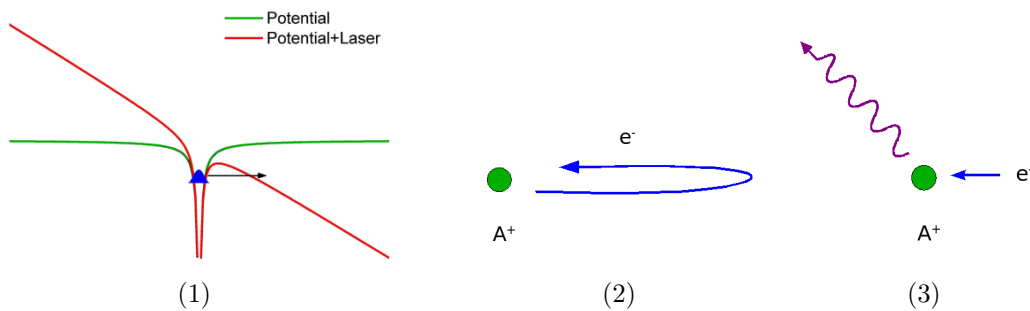


Figure 2.1: *The three steps of HHG: (1) The laser superposes with the coulomb potential of the ionic core, creating a finite potential wall. Thus the atom can ionize when its outer electron tunnels through this barrier. (2) The electron is accelerated in the strong electric field. (3) When the ion and the electron recombine, a XUV photon is emitted.*

In the first step, where the atom ionizes, the electron has to tunnel through a coulombic barrier. The height of this barrier is characterized by the ionization potential  $I_p$ , therefore the condition  $\hbar\omega_0 \ll I_p$  implies that the absorption of many photons is necessary to ionize the atom. Generally, this multi-photon process has to be described by a quantum-mechanical model, but in the high-energy regime, a quasistatic approximation of the process is sufficient for most applications. Note, that this approximation partly neglects the photonic character of the light field [15]. Several quasistatic models were invented to describe and simulate the strong field atom ionization via a tunneling process. In these models the atom is considered as an electron bound in the coulomb potential of the atomic core (ion), see figure 2.1.1 (green line). The intense laser field is simply described as a slowly oscillating electric field  $\vec{E}(t) = \vec{E}_0(t) \cos(\omega_0 t)$  whose interaction potential,  $e\vec{E}\vec{r}$ , superposes with the coulomb potential of the core and creates a finite tunneling barrier in the direction of the laser (red line). When the laser field is strong enough, there is some probability for the electron to escape the atom by tunneling through the barrier.

A widely used formula for this process was derived by Ammosov, Delone and Krainov [16]. This so-called ADK rate agrees well with the experimental

results. Also the assumptions made in this model, a classical electric laser field and tunneling from a discrete state into the continuum, have been proven by measurements of structureless photoelectron spectra in this regime [15].

In the ADK theory the instantaneous ionization rate in S.I. units is [15, 16]

$$w(t) = \omega_p |C_{n^*}|^2 \left( \frac{4\omega_p}{\omega_t} \right)^{2n^*-1} \exp \left( -\frac{4\omega_p}{3\omega_t} \right), \quad (2.3)$$

with

$$\omega_p = \frac{I_p}{\hbar}, \quad \omega_t = \frac{e|E_1(t)|}{\sqrt{2m_e I_p}}, \quad n^* = Z \left( \frac{I_{ph}}{I_p} \right)^{1/2},$$

$$|C_{n^*}|^2 = \frac{2^{2n^*}}{n^* \Gamma(n^* + 1) \Gamma(n^*)}.$$

$|E_1(t)|$  is the amplitude of the electric field,  $Z$  the resulting net charge of the atom,  $I_p$  the ionization potential of the irradiated atom and  $I_{ph}$  the ionization potential of hydrogen.  $\Gamma(x)$  denotes the mathematical Gamma function.

The double logarithmic plot in figure 2.2 shows the dependance of the ionization rate  $w(t)$  on the local intensity of the laser field  $I(t) = \epsilon_0 c |E(t)|^2$ . The ADK rate dramatically rises for intensities much higher than  $10^{14} \text{W/cm}^2$ , thus the depletion of the ground state should be taken into account at least for the upper level of the parameter regime of the HHG process.

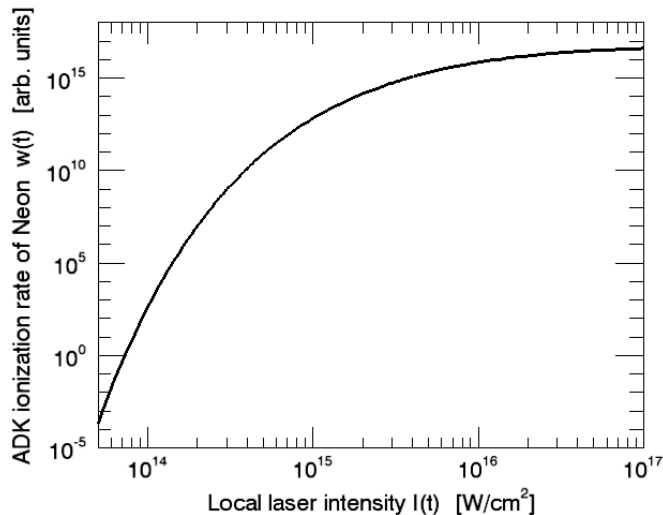


Figure 2.2: Double logarithmic plot of the instantaneous tunneling ionization rate  $w(t)$  of Neon vs. the laser intensity  $I(t) = \epsilon_0 c |E(t)|^2$ .

For a slowly varying pulse envelope approximation, one might average the ionization rate over one optical cycle of the laser field and obtain

$$w_{avg}(t) = \left( \frac{3\omega_p}{2\pi\omega_t} \right)^{1/2} w(t) . \quad (2.4)$$

The ionization rate allows for an estimate of the probability of an atom to have remained in its groundstate

$$R(t) = \exp \left[ - \int_{-\infty}^t w(t') dt' \right] . \quad (2.5)$$

Hence, the free-electron density inside the gas, which has to be equal to the density of ions is given by

$$n_e(t) = n_0 \{1 - R(t)\} , \quad (2.6)$$

where  $n_0$  denotes the neutral atom density and one-electron ionization is considered only.

After ionization, when the electron appears in the continuum, it will immediately be accelerated in the strong laser field. Neglecting the core attraction, thus considering a free electron and presuming a linear polarized laser field in x-direction, the classical electron motion is described by:

$$m \frac{\partial^2 x}{\partial t^2} = eE(t) . \quad (2.7)$$

Solving this differential equation within the slowly varying envelope approximation (i.e.  $E(t) \approx E \cos(\omega_0 t)$ ) and assuming zero initial velocity leads to a time dependant electron velocity of

$$v(t) = \frac{eE}{m_e \omega_0} (\sin(\omega_0 t) - \sin(\omega_0 t_i)) , \quad (2.8)$$

and the ponderomotive potential of the electron in the laser field as its classical mean kinetic energy,

$$U_p = \langle \frac{1}{2} m_e v^2 \rangle = \frac{e^2 E^2}{4m_e \omega_0^2} . \quad (2.9)$$

The above equations state, that the velocity  $v(t)$  of an electron strongly depends on the time of ionization  $t_i$ . A numerical investigation of the velocity of the electrons at their first return to the parent ion in dependance on the ionization time was performed to calculate the maximum gained energy available for the HHG process. The result of this calculation is shown in figure 2.3, where the clas-

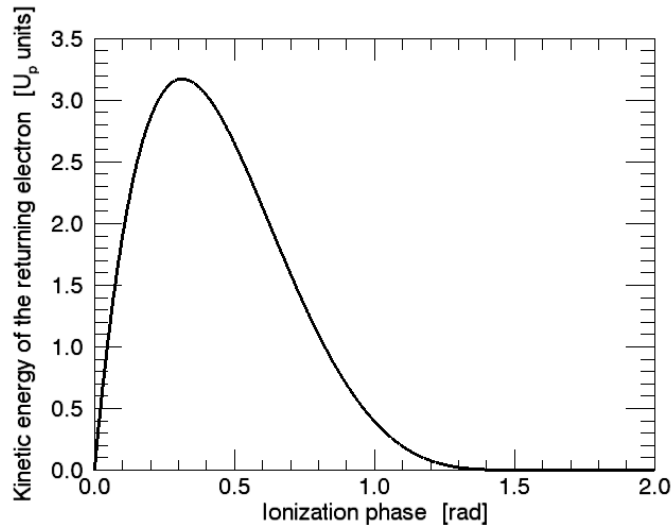


Figure 2.3: Plot of the kinetic energy of an electron at its first return to the nucleus against the ionization phase  $\omega_0 t_i$ .

sical kinetic energy of the returning electron is plotted against its ionization phase  $\omega_0 t_i$ . The maximum electron energy and the corresponding phase of ionization to produce the highest photon energies within the HHG process read as

$$E_{kin,max} = 3.17 U_p \quad \text{at} \quad \omega_0 t_i = 0.310 . \quad (2.10)$$

The maximum frequency  $\omega_c$  in a HHG spectrum is linked to the maximum energy which the electron radiates when recombining, thus to its kinetic energy and to the binding-energy gained while tunneling. Hence, an estimate of a key parameter of the HHG process, the position of the cut-off in the spectra is given by the *cut-off law*:

$$\hbar\omega_c = I_p + 3.17U_p. \quad (2.11)$$

The cut-off law clarifies, that the maximum harmonic frequency achievable from the HHG process is strongly linked to the ponderomotive potential  $U_p$  and thus to the field amplitude and the wavelength of the fundamental laser light.

This implies the following laws [4]:

- The higher the intensity of the laser and thus  $U_p$ , the higher the cut-off frequency.
- The larger the wavelength of the fundamental, the higher the cut-off frequency.
- The higher the ionization potential  $I_p$ , the higher the cut-off frequency.

Note, that not only the cut-off law, but also some other interesting limits on the HHG process are explained by the Simple Man Model. For instance, HHG will only occur if the driving laser field is linearly polarized. Ellipticity on the laser beam causes the returning electron to 'miss' the parent nucleus. Quantum mechanically, the overlap of the returning electron wavepacket and the nuclear wavepacket is reduced. This has been observed in experiments, where the intensity of harmonics has decreased rapidly with increasing ellipticity [15].

Another effect which limits the intensity of the driving laser is the Lorentz force. At intensities above  $\sim 10^{16} \text{ W/cm}^2$  the magnetic component of the laser pulse which is ignored in weak field optics, can become strong enough to deflect the returning electron. This will also reduce the overlap between the wavepackets of the electron and the parent nucleus and hence prevent the generation of higher harmonics.

HHG is a stochastic process, where the atom has a strong probability to be ionized every half optical cycle of the fundamental laser, when the electric field is maximal. Therefore, the periodicity of the HHG process is given by  $T_0/2$ .

Furthermore, as it will be described in the next section, the electron has to be considered as a quantum mechanical wave packet, which undergoes a transition from a bound state to a continuum state at a certain time  $t_i$ , evolves in the laser field and finally descends to the bound state again under radiation of the kinetic energy gained while propagating through the continuum. This quantum wave packet oscillates with its own frequency, however the total phase, the electron accommodates and therefore the phase of the occurring XUV radiation is strongly linked to the time of ionization and to the strength of the fundamental. Thus the phase of the electronic wave packet at recombination and therefore the phase of the XUV light are locked to the phase and the amplitude of the fundamental laser beam. This influences the collective behavior in the spatial domain, since spatial coherence properties of the irradiating laser are partly transferred to the harmonic emission. Hence, HHG is a spatial coherent process due to the fact that atoms irradiated by the same electric field will produce the same XUV light. The total emitted field in a macroscopic medium is given by a sum over the emissions from many atoms. Thus not only the single atom response, but also collective effects as phase matching or reabsorption of the XUV light determine the net intensity of the generated harmonics [15]. Phase matching is given, if the radiation generated by different atoms at different positions in the medium interferes constructively at the exit of the medium. For a perfect match of phases, this condition reads

$$\Delta\mathbf{K} = 0 \tag{2.12}$$

or, for approximate phase matching

$$\Delta\mathbf{K} \mathbf{L}_{\text{med}} < \pi , \tag{2.13}$$

where  $\mathbf{L}_{\text{med}}$  describes the length and direction of the medium and  $\mathbf{K} = \mathbf{k}_q - q\mathbf{k}_0$  denotes the mismatch between the wavevectors of the harmonic and the fundamental light. The dependance of the harmonic phase on the intensity of the laser can be written as  $\varphi_q = \alpha_q I$  [15], thus an additional wavevector  $\mathbf{k}_I = -\nabla(\alpha_q I)$  enters the phase mismatch, resulting in a generalized phase matching condition for HHG with

$$\Delta\mathbf{K} = \mathbf{k}_q + \mathbf{k}_I - q\mathbf{k}_0 . \quad (2.14)$$

The presence of only odd harmonics in the measured spectra can be explained by considerations on the periodicity of the process. The coulomb potential of the atomic core is symmetric, hence tunneling can happen twice an optical cycle for both signs of the laser electric field, resulting in a periodicity for the harmonic emission of half an optical cycle,  $T_0/2$ . But due to the fact, that the harmonic emission is phase locked to the fundamental laser, the alternating sign of the laser makes the real periodicity  $T_0$  with an antiperiodicity of  $T_0/2$ . However, the periodicity in intensity is still  $T_0/2$ .

The field emitted for a specific harmonic  $\omega_q$  within half a laser cycle may be written as a wave with frequency  $\omega_q = q\omega_0$  and complex amplitude  $A(\omega_q)$ ,

$$E_0(\omega_q, t) = A(\omega_q) \exp -i(\omega_q t + \varphi_q) . \quad (2.15)$$

Then, the total emitted field after  $N$  half optical cycles, including periodicity, reads

$$\begin{aligned} E(\omega_q, t) &= \sum_{n=1}^N (-1)^n E_0(\omega_q, t_n) \\ &= \sum_{n=1}^N (-1)^n A(\omega_q) \exp -i(\omega_q(t - nT_0/2) + \varphi_q) \\ &= A(\omega_q) \exp -i(\omega_q t + \varphi_q) \sum_{n=1}^N \exp +in(\omega_q T_0/2 - \pi) \\ &= E_0(\omega_q, t) \sum_{n=1}^N \exp +in(\omega_q T_0/2 - \pi) , \end{aligned} \quad (2.16)$$

with  $n$  indexing bygone half periods  $T_0/2$  and  $t_n = t - nT_0/2$ . Thus the total emission corresponds to the signal generated during one half optical cycle multiplied by an additional time-dependant amplitude. Reshaping this amplitude results in

$$\sum_{n=1}^N \exp +in(\omega_q T_0/2 - \pi) = \frac{1 - e^{iN(\omega_q T_0/2 - \pi)}}{e^{-i(\omega_q T_0/2 - \pi)} - 1} . \quad (2.17)$$

This expression shows, that the total amplitude of the harmonic emission for many optical cycles  $N$  will become macroscopic only if the denominator vanishes, thus

$$\exp[-i(\omega_q T_0/2 - \pi)] = 1 . \quad (2.18)$$

Hence, one gets

$$(2n - 1)\pi = \frac{\omega_q T_0}{2} = q \frac{\omega_0 T_0}{2} = q\pi$$

$$\implies \omega_q = (2n + 1)\omega_0 \quad , \quad \forall n \in \mathbb{N} . \quad (2.19)$$

Note, that these considerations are valid only, if the depletion of the ground state is negligible and the amplitude of the laser is approximately constant. Thus, the constraint in (2.19) on the harmonic spectra does neither hold for very short pulses nor for such high intensities, that the groundstate is depleted.

## 2.2 Strong Field Approximation

The *Lewenstein Model* [4], also called the *Strong Field Approximation* (SFA), is a fully quantum mechanical approach which describes the HHG process. The basic equation of this theory is the time dependent Schrödinger equation (TDSE)

$$i|\dot{\Psi}(\vec{r}, t)\rangle = \left[ -\frac{1}{2}\hat{\nabla}^2 + \hat{V}(\mathbf{x}) - E(t) \hat{x} \right] |\Psi(\vec{r}, t)\rangle , \quad (2.20)$$

with the coulombic core potential operator  $\hat{V}(\mathbf{x})$  and the dipole operator consisting of the laser electric field  $E(t)$  times the space operator  $\hat{x}$ . For convenience, modified atomic units are used, where additionally all energies are expressed in terms of the energy of a fundamental photon, thus defining  $\hbar = e = m_e = c = \epsilon_0 = \omega_0 = 1$ . With the help of the TDSE one obtains the induced dipole moment

$$x(t) = \langle \Psi(\vec{r}, t) | \hat{x} | \Psi(\vec{r}, t) \rangle , \quad (2.21)$$

which is directly linked to the high frequency spectra produced within the HHG process.

In the following only linearly polarized light is considered, and the model is restricted to one electron ionization. Additionally this approach is confined to the case, where  $I_p \gg 1$  (typically  $I_p \approx 5 - 20$  laser photons). The ponderomotive potential  $U_p$  should be in the range or larger than  $I_p$ , but still below the saturation energy  $U_{sat}$ , where all the gas atoms ionize during the interaction with the laser. For these parameters, tunneling theories, for instance, the ADK model [16],

become valid. Because the laser intensity is as high as  $10^{14}$ - $10^{15}$   $W/cm^2$ , one can also neglect any occurring intermediate resonances.

When the tunneling process emerges, the electron is lifted from the ground-state  $|0\rangle$  up to a continuum state  $|\mathbf{v}\rangle$ , denoted by its kinetic momentum. Once it has appeared in the continuum, the interaction of the electron and the laser is determined by the last term of the the Hamiltonian,  $E(t)\hat{x}$ . Assuming, that continuum to continuum (C-C) transitions do not contribute to the HHG process, the expectation value of the dipole moment with respect to transitions between to continuum states reads

$$\langle \mathbf{v} | \hat{\mathbf{x}} | \mathbf{v}' \rangle = -\mathbf{i} \langle \mathbf{v} | \nabla_{\mathbf{v}} | \mathbf{v}' \rangle \approx -\mathbf{i} \nabla_{\mathbf{v}} \delta(\mathbf{v} - \mathbf{v}') . \quad (2.22)$$

However, the neglected non-diagonal parts of the C-C transition matrix might be systematically added up by means of perturbation theory [4].

In eq.(2.20), the second term of the Hamiltonian represents the interaction of the electron and the atomic core potential  $V(\mathbf{r})$ . This term is negligible, because when the electron appears in the continuum it is immediately accelerated by the intense laser field. At the outer point of the electron trajectory, the kinetic energy of the electron is relatively low, but for these distances the core attraction vanishes also. Lastly, when the electron returns to the nucleus, it has gained such a high momentum, that again atomic potential forces can be neglected.

This can formally be written as

$$\langle \mathbf{v}' | \hat{V}(\mathbf{r}) | \Psi \rangle \approx 0 . \quad (2.23)$$

The above considerations suggest that the following assumptions are valid in this regime of parameters [4].

- (a) The contribution to the evolution of the system of all bound states except the ground state  $|0\rangle$  can be neglected.
- (b) The depletion of the ground state can be neglected ( $U_p < U_{sat}$ ).
- (c) In the continuum, the electron can be treated as a free particle moving in the electric field with no effect caused by the atomic core potential  $V(\mathbf{x})$ .

Assumption (b) is only valid, if the laser intensity is not too high (i.e.  $U_p < U_{sat}$ ), otherwise the depletion of the groundstate has to be taken into account. Provided, that  $U_p$  is large enough, (c) does not only hold for short range potentials, but also for long range potentials, as of hydrogen-like atoms. Assumption (c) implies, that the electron has gained such a large kinetic energy when returning to the nucleus, that the atomic core attraction is negligible. This is not the case for lower harmonics of the order of  $2q + 1 \leq I_p / (\hbar\omega_0)$ . Therefore the Lewenstein Model is only applicable for higher harmonics with photon energies  $\hbar\omega_q \geq I_p$ . In general, assumptions (a)-(c) are justified, if the so-called *Keldysh parameter*

$\gamma = \sqrt{I_p/2U_p}$  is smaller than one [4], thus  $I_p < 2U_p$ .

In the following a formula, which approximately describes the induced dipole moment of the atom for the above discussed regime of parameters is derived by solving the time-dependent Schrödinger equation (2.20).

To solve this differential equation one has to make a conclusive Ansatz. The considerations (a)-(c) motivate an approach, where the time-dependent wave function is split into two parts, the bound part represented only by the ground-state  $a(t)|0\rangle$  and an integral over all unbound continuum states  $b(\mathbf{v}, t)|\mathbf{v}\rangle$ ,

$$|\Psi\rangle = e^{iI_p t} \left( a(t)|0\rangle + \int d^3\mathbf{v} b(\mathbf{v}, t)|\mathbf{v}\rangle \right). \quad (2.24)$$

The prefactor in equation (2.24) represents the free oscillations of the ground-state with the depth of the potential  $I_p$  as bare frequency. Its amplitude is set to  $a(t) \approx 1$ ,  $\dot{a}(t) \approx 0$  in the following, as claimed in assumption (b). Thus, to solve eq. (2.20) one has to find an expression for the amplitudes of the continuum states  $b(\mathbf{v}, t)$ . They are defined by a Schrödinger type equation, see also appendix A,

$$\dot{b}(\mathbf{v}, t) = -i \left( \frac{\mathbf{v}^2}{2} + I_p \right) b(\mathbf{v}, t) - E(t) \frac{\partial b(\mathbf{v}, t)}{\partial v_x} + iE(t) d_x(\mathbf{v}). \quad (2.25)$$

In the above equation  $\mathbf{d}(\mathbf{v}) = \langle \mathbf{v} | \mathbf{x} | 0 \rangle$  denotes the atomic dipole matrix element for bound-free transitions of electrons, which is later determined by the shape of the core potential. Because only linear polarized light is considered, w.l.o.g.  $\vec{x}$  can be chosen as the polarization axis, i.e. only the  $x$ -component  $d_x(\mathbf{v})$  of the dipole matrix element enters the expression for  $b(\mathbf{v}, t)$ . Thus, the whole information about the atom is reduced to the form of  $\mathbf{d}(\mathbf{v})$ , and its complex conjugate  $\mathbf{d}^*(\mathbf{v})$  [4].

The differential Schrödinger type equation (2.25) can be solved exactly [4], leading to a closed form of  $b(\mathbf{v}, t)$ , using the laser  $E(t)$  and the corresponding vector potential  $\mathbf{A}(t) = \int_{-\infty}^t E(t') dt'$ :

$$b(\mathbf{v}, t) = i \int_0^t dt' E(t') d_x(\mathbf{v} + \mathbf{A}(t) - \mathbf{A}(t')) \\ \times \exp \left\{ -i \int_{t'}^t dt'' [(\mathbf{v} + \mathbf{A}(t) - \mathbf{A}(t''))^2 / 2 + I_p] \right\}. \quad (2.26)$$

Thus, the expectation of the position of the electron which is equal to the induced dipole moment, eq.(2.21), can be rewritten as

$$x(t) = \int d^3\mathbf{v} d_x^*(\mathbf{v}) b(\mathbf{v}, t) + c.c. . \quad (2.27)$$

In a next step a change of variables to the canonical momentum  $\mathbf{p} = \mathbf{v} + \mathbf{A}(t)$  is performed and the quasiclassical action is introduced.

The quasiclassical action

$$S(\mathbf{p}, t, t') = \int_{t'}^t dt'' \left( \frac{[\mathbf{p} - \mathbf{A}(t'')]^2}{2} + I_p \right) \quad (2.28)$$

describes the motion of a freely moving electron in the laser electric field. Hence an additional phase factor  $\exp[-iS(\mathbf{p}, t, t')]$  enters the expression for the dipole moment. Note that eq. (2.28) also takes into account some effects on the phase of the electronic wave packet due to the depth of the binding core potential (i.e. the ionization potential  $I_p$ ). However, as it is just an additional constant, it neglects other perturbations of the electronic wave function due to the atomic potential  $V(x)$ . This means that the canonical momentum  $\mathbf{p}$  is an observed quantity inbetween the time of ionization  $t'$  and the time of recombination  $t$ .

The expression for the induced dipole moment now reads as

$$x(t) = i \int_0^t dt' \int d^3\mathbf{p} \quad d_x [\mathbf{p} - \mathbf{A}(t')] \times E(t') \\ \times \quad d_x^* [\mathbf{p} - \mathbf{A}(t)] \times e^{-iS(\mathbf{p}, t, t')} + c.c. \quad (2.29)$$

There is a rather intuitional physical interpretation of equation (2.29) as a continuous sum of probability amplitudes, which in principal corresponds to the three steps of HHG described in the Simple Man Model. The first term,  $d_x [\mathbf{p} - \mathbf{A}(t')] \times E(t')$ , represents the probability amplitude for the electron to perform a transition from the ground state to the continuum at a time  $t'$ . During its flight, the electron is considered as a particle moving freely in the laser electric field and therefore the wavefunction describing the electron acquires an additional phase factor  $\exp(-iS(\mathbf{p}, t, t'))$ . The last term in eq.(2.29), the complex-conjugate of the dipole matrix element  $d_x^* [\mathbf{p} - \mathbf{A}(t)]$ , can be interpreted as the probability amplitude for a recombination of the electron and the atomic core to happen at time  $t$ .

An alternative, but slightly unintuitive interpretation of equation (2.29) is a time-reversed process, where the electron appears in the continuum at a time  $t$  in the future, propagates back to  $t'$  and recombines with the nucleus. This interpretation allows for the invariance with respect to time included in the basic equation of this model, the TDSE (2.20).

The integral over the continuum states in eq. (2.29) can be approximately resolved via a stationary phase method, see appendix B, thus yielding a numerically computable expression for the laser induced atomic dipole moment,

$$x(t) = i \int_0^\infty d\tau \left( \frac{\pi}{\epsilon + i\tau/2} \right)^{3/2}$$

$$\begin{aligned}
 & \times d_x [p_{st}(t, \tau) - A_x(t - \tau)] E(t - \tau) \\
 & \times d_x^* [p_{st}(t, \tau) - A_x(t)] \\
 & \times \exp[-iS_{st}(t, \tau)] \\
 & + \text{c.c.} .
 \end{aligned} \tag{2.30}$$

In the above equation, the linear polarization of the laser was taken into account by writing  $A_x(t)$  instead of the whole vector potential  $\mathbf{A}(t)$  and the time coordinate has been substituted by the *time of flight* of the electron:  $\tau = t - t'$ . Due to the integration method, the canonical momentum  $\mathbf{p}$  and the quasiclassical action  $S(\mathbf{p}, t, t')$  have been replaced by their stationary values

$$p_{st}(t, \tau) = \frac{1}{\tau} \int_{t-\tau}^t dt' A(t') , \tag{2.31}$$

$$S_{st}(t, \tau) = (I_p - \frac{1}{2} p_{st}^2) \tau + \frac{1}{2} \int_{t-\tau}^t dt' A^2(t') . \tag{2.32}$$

The additional prefactor in eq.(2.30),  $[\pi/(\epsilon + i\tau/2)]^{3/2}$ , with an infinitesimal regularization constant  $\epsilon$ , has arisen from the integration over all continuum states. It incorporates the spread of the electronic wave function due to quantum diffusion during the propagation in the continuum. Because of its proportionality to  $\tau^{-3/2}$ , it limits the electrons contributing to the HHG process to those only, which return after a few laser cycles.

## 2.3 Propagation in the Medium

In the previous sections the HHG process was contemplated only under the perspective of one single atom irradiated by the laser. In order to get a description which is closer to the real experimental situation, one has to include the propagation of the laser and the generated harmonics through the gas medium.

For convenience, radial symmetry is assumed for the fundamental laser beam and for the induced harmonic light in the present work, which implies the use of cylindrical coordinates for the equations describing the evolution of the light fields.

The source term of the propagation equation is characterized by the single-atom response. Using the index  $i \in \{1, q\}$ , denoting the fundamental, respectively the harmonic electro-magnetic field, the differential equation describing the evolution reads

$$\nabla^2 E_i(r, z', t') - \frac{1}{c^2} \frac{\partial^2 E_i(r, z', t')}{\partial t'^2} = G_i(r, z', t') , \tag{2.33}$$

where  $G_i(r, z', t')$  is the designated source term,  $z'$  the propagation and  $r'$  the transverse coordinate. Transforming the above equation to a moving frame ( $z =$

$z'$  and  $t = t' - z'/c$ ) and applying the paraxial approximation (i.e. using  $\frac{\partial^2 E}{\partial z^2} \approx 0$ ) leads to

$$\nabla_{\perp}^2 E_i(r, z, t) - \frac{2}{c} \frac{\partial^2 E_i(r, z, t)}{\partial z \partial t} = G_i(r, z, t) . \quad (2.34)$$

This approximation is valid for beam sizes significantly larger than the wavelength and does not limit the pulse duration [17].

The temporal derivative in equation (2.34) is eliminated by performing a Fourier transform, yielding a diffusion-type equation

$$\nabla_{\perp}^2 \tilde{E}_i(r, z, \omega) - \frac{2i\omega}{c} \frac{\partial \tilde{E}_i(r, z, \omega)}{\partial z} = \tilde{G}_i(r, z, \omega) , \quad (2.35)$$

where

$$\begin{aligned} \tilde{E}_i(r, z, \omega) &= \hat{F}^+ [ E_i(r, z, t) ] , \\ \tilde{G}_i(r, z, \omega) &= \hat{F}^+ [ G_i(r, z, t) ] , \end{aligned}$$

with the Fourier transform operator  $\hat{F}^+$  acting on the time coordinate.

To obtain a full set of equations describing the propagation through a gascell, the source terms  $G_i(r, z, t)$  have to be determined. Linear gas dispersion and depletion of the laser are not considered for the source of the fundamental beam, since they are negligible in the underlying regime of parameters. However, temporal plasma-induced phase modulations and spatial plasma lensing effects are taken into account and lead to:

$$\begin{aligned} G_1(r, z, t) &= \frac{\omega_p^2(r, z, t)}{c^2} E_1(r, z, t) \\ \implies \tilde{G}_1(r, z, \omega) &= \hat{F}^+ \left[ \frac{\omega_p^2(r, z, t)}{c^2} E_1(r, z, t) \right] . \end{aligned} \quad (2.36)$$

Where

$$\omega_p^2(r, z, t) = \frac{e^2 n_e(r, z, t)}{\epsilon_0 m_e} \quad (2.37)$$

is the squared plasma frequency with the electron density  $n_e(r, z, t)$  calculated from the ADK instantaneous ionization rate, see eq. (2.6).

Within the harmonic source term, the formation of the harmonics is introduced via the non-linear polarization  $P_{nl}$ . But effects of free electron dispersion are neglected due to the fact, that the high-order harmonic light consists of frequencies much higher than the plasma frequency.

Hence, one obtains

$$\begin{aligned}
 G_q(r, z, t) &= \mu_0 \frac{\partial^2 P_{nl}(r, z, t)}{\partial t^2} \\
 \implies \tilde{G}_q(r, z, \omega) &= -\mu_0 \omega^2 \tilde{P}_{nl}(r, z, t) ,
 \end{aligned} \tag{2.38}$$

with

$$\begin{aligned}
 P_{nl}(r, z, t) &= [n_0 - n_e(r, z, t)] R(r, z, t) x(r, z, t) \\
 &= n_0 R^2(r, z, t) x(r, z, t) .
 \end{aligned} \tag{2.39}$$

Here, the atomic dipole moment  $x(r, z, t)$ , eq. (2.21), calculated within the SFA is multiplied by the probability of an atom to have remained in its groundstate  $R(r, z, t)$ , eq. (2.5), to allow for the depletion of the ground state, which was neglected in the Lewenstein Model. This probability also occurs in the expression for the electron density, eq. 2.6, therefore it enters the harmonic source twice.

Note, that in the above equation no slowly varying envelope approximation in time was performed, thus taking the whole pulse into account and therefore giving no limits for the pulse duration due to approximations.

Once the above propagation equations are solved, one can easily obtain the power spectrum of the harmonics by integrating over the transverse direction at a certain point of interest  $z_1$ .

$$I_q(\omega) \propto \int_0^\infty |\tilde{E}_q(r, z_1, \omega)|^2 2\pi r dr. \tag{2.40}$$

---

# 3

## HHG Simulation

---

The subject of this work was to investigate the HHG radiation as a source for the BESSY Soft X-ray FEL. For an adequate treatment of the HHG source in this context, a HHG simulation tool, which uses a three-dimensional propagation model is mandatory. As such a simulation program was not available, a 3D code which is valid within the tunneling regime of parameters was developed. This chapter deals with the implementation of this simulation code, called  $\mathcal{R}$ HYNO.

Before implementing the code, basic simulation parameters like the temporal and the spatial discretization have to be determined and technical questions like how to keep the fields in storage and how to numerically implement the underlying mathematical model have to be answered.

The first part of this chapter addresses the main assumptions and the basic numerical methods of the developed simulation program. The second section deals with the calculation of the single atom spectra, whereas the numerical solution of the propagation equations is explained in section 3. In the last part of this chapter, an overview of the simulation sequence and its parameters is given. All computational methods used in this chapter, can be found in textbooks, like [18].

### 3.1 Assumptions and Numerical Methods

The simulation is based on a cylindrical symmetric spatial geometry and restricted to laser beams with radial symmetry.

As the program is written in  $C^{++}$ , the fields are kept in a special  $C^{++}$ -class, which holds a complex-vector  $E_j(t_j)$ , or  $\tilde{E}_j(\omega_j)$  respectively for every  $0 \leq r_i \leq r_{max}$  and provides methods to Fourier transform the fields from time to frequency domain and vice versa. Additionally the corresponding  $\omega$ -,  $t$ - and  $r$ -axis are saved in this data structure, thus completely describing the fundamental or the harmonic light at a certain point along the propagation axis  $z$ . During the simulation all functions and fields are calculated on a  $t/\omega$ - and a  $r$ -grid, thus there is no direct information on the field values inbetween the grid points. But, as the gridwidth is chosen rather small compared to the wavelength, they can be linearly interpolated, if needed. Note, that the fields are kept in memory only for the actual point  $z_n = n\Delta z$  along the propagation axis, not for any bygone  $z_{n'}$ .

*Discrete Fourier Transforms* (DFT) are a common method in computational sciences. They allow for Fourier transformations of signals and functions which

are not analytically known or integrable. When setting up the number of temporal grid points a fundamental law for Discrete Fourier Transforms has to be taken into account, which links the number of points in time and the sampling interval  $\delta t$  with the resolution and the maximum frequency in the sampled spectra. The maximum frequency being sampled by a DFT is given by Nyquist's sampling theorem [18]

$$\omega_c = \frac{\pi}{\delta t}. \quad (3.1)$$

If the signal to be transformed contains higher frequencies than  $\omega_c$ , the resulting spectrum is aliased. This means that contributions from higher frequencies are folded back into the lower part of the spectrum, thus it is important to prevent aliasing by choosing the parameters such, that there are no contributions from frequencies higher than  $\omega_c$ .

Considering the HHG process, it is useful to define the maximum sampling frequency as  $\omega_c = Q\omega_0$ , where  $Q$  denotes the number of the highest harmonic to be sampled. This gives us an estimate for the size of the necessary sampling interval

$$\delta t = \frac{\pi}{Q\omega_0}. \quad (3.2)$$

Equation (3.2) shows, that the higher  $\omega_c$ , the smaller  $\delta t$  and therefore, the smaller the considered total time interval  $T = (N - 1)\delta t$ . However, there is a limit for the minimum time interval  $T$ , as it has to be long enough to cover the whole laser pulse. On the other hand, due to computation speed, to save and handle more points in time than necessary is not desirable. Therefore the parameter  $L$  is introduced, which represents the minimum multiple of pulse durations  $\tau$ , defined as FWHM, which should fit into the total length of the temporal grid  $T$ .

$$T \geq L\tau \quad (3.3)$$

From equations (3.2) and (3.3) one can determine the minimum number of points in time needed to properly run a simulation with a fundamental laser beam of pulse duration  $\tau$  and frequency  $\omega_0$ .

$$\begin{aligned} T &= (N - 1)\delta t \geq L\tau \\ \implies N - 1 &\geq \frac{L\tau}{\delta t} = \frac{LQ\omega_0\tau}{\pi} \end{aligned} \quad (3.4)$$

The code uses  $L = 3$  and  $Q = 300$  as default parameters which give good unaliased results for most of the HHG simulation cases.

From the maximum frequency and the number of points in time one can also determine the frequency discretization interval  $\delta\omega$ . In DFTs the frequency range spans from  $-\omega_c + \delta\omega$  to  $+\omega_c$ , hence

$$\delta\omega = \frac{2\omega_c - \delta\omega}{N - 1}$$

$$\implies \delta\omega = \frac{2\omega_c}{N} = \frac{2\pi}{N\delta t} = \frac{2Q\omega_0}{N} . \quad (3.5)$$

## 3.2 Single Atom Spectra

The core of this HHG simulation is the calculation of the single atom spectra on the basis of the Lewenstein approximation eq. (2.30)

$$\begin{aligned} x(t) = & i \int_0^\infty d\tau \left( \frac{\pi}{\epsilon + i\tau/2} \right)^{3/2} \\ & \times d[p_{st}(t, \tau) - A(t - \tau)] E_1(t - \tau) \\ & \times d^*[p_{st}(t, \tau) - A(t)] \\ & \times \exp[-iS_{st}(t, \tau)] \\ & + \text{c.c.} , \end{aligned} \quad (3.6)$$

where  $\epsilon$  is a positive, infinitely small regularization constant [eg.  $10^{-16}$ , see also comment on eq.(B.15)] and  $E_1(t)$  the electric field of the linear polarized laser beam.  $A(t)$  denotes the corresponding vector potential, which in atomic units is defined as

$$A(t) = \int_{-\infty}^t E(t') dt' . \quad (3.7)$$

The dipole matrix element  $d(p)$  in eq. (3.6) describes transitions between the ground state and the continuum. For hydrogen-like atoms, it can be approximated as [4]

$$d(p) = i \frac{2^{7/2}(2I_p)^{5/4}}{\pi} \frac{p}{(p^2 + 2I_p)^3} . \quad (3.8)$$

$S_{st}$  and  $p_{st}$ , given in equations (2.32) and (2.31), are the stationary values of the quasiclassical action and the canonical momentum

$$p_{st}(t, \tau) = \frac{1}{\tau} \int_{t-\tau}^t dt' A(t') , \quad (3.9)$$

$$S_{st}(t, \tau) = (I_p - \frac{1}{2} p_{st}^2) \tau + \frac{1}{2} \int_{t-\tau}^t dt' A^2(t') . \quad (3.10)$$

Within the simulation code, the integrals for  $x(t)$ ,  $A(t)$ ,  $p_{st}(t, \tau)$  and  $S_{st}(t, \tau)$  are performed using the repeated *Simpson* rule [18]. Therefore the functions are piecewise interpolated by parabolas, whose antiderivative is known analytically. This method is fourth-order accurate in time and reads

$$\begin{aligned} I &= \int_{t_0}^{t_0+N\delta t} f(t) dt \\ &= \frac{\delta t}{3} \left[ f_0 + \sum_{j=1}^{(N-2)/2} \left( 4f_{2j-1} + 2f_{2j} \right) + 4f_{N-1} + f_N \right] + \mathcal{O}(\delta t^4), \end{aligned} \tag{3.11}$$

for an even number of interpolation points  $N$ . In case of an odd  $N$ , the first interval between  $t_0$  and  $t_1$  is interpolated by a straight line according to the trapezoidal integration rule.

### 3.3 Propagation

In this section a numerical implementation of the propagation equation (2.35) and its solution are presented and a stability analysis of the underlying differencing scheme is discussed.

#### 3.3.1 Solving the Propagation Equation

Equation (2.35) is a diffusion type equation and can be rewritten in the concise form,

$$\frac{\partial u}{\partial z} = D [\nabla_{\perp}^2 u - S] , \tag{3.12}$$

where  $D = c/2i\omega$  denotes the diffusion constant,  $S = S(r, z, \omega)$  is the source of the field and  $u = u(r, z, \omega)$  represents the diffusing field itself.

The Laplacian in the above equation only acts on components perpendicular to the direction of propagation  $z$ . This motivates the use of a cylindrical coordinate system  $(r, \varphi, z)$ . Note, that the simulation only allows for fully radial symmetric fields, with vanishing derivatives with respect to  $\varphi$ , yielding

$$\nabla_{\perp}^2 u = \left[ \frac{\partial^2}{\partial r^2} + \frac{1}{r} \frac{\partial}{\partial r} \right] u . \tag{3.13}$$

For numerical simulations, space has to be discretized. The simplest method

---

is to split the region of interest into  $N$  grid points  $r_j$  equally separated by

$$\Delta r = r_j - r_{j-1} = \frac{R_{max}}{N-1} . \quad (3.14)$$

Now the field and the sources can be represented as independant vectors for any frequency  $\omega_k$ :

$$\begin{aligned} u_j^n(\omega_k) &:= u(r_j, z_n, \omega_k) \\ S_j^n(\omega_k) &:= S(r_j, z_n, \omega_k) , \end{aligned} \quad (3.15)$$

with  $r_j = j\Delta r$  and  $z_n = n\Delta z$ , respectively. The index  $n$  indicates the  $n$ th integration step along the  $z$ -axis of width  $\Delta z$ , whereas  $\omega_k$  denotes the corresponding frequency slice. Due to the structure of the propagation equation, it can be solved independantly for any slice without any effect on other slices. In the following the explicit notation of  $\omega_k$  is omitted.

The next step is to find the discretized form of the Laplacian in polar coordinates. Expressions for the first and the second order derivative in the polar Laplacian can be found using Taylor approximations around the points of interest, leading to:

$$\begin{aligned} \left( \frac{\partial}{\partial r} u \right)_{j>0} &= \frac{u_{j+1} - u_{j-1}}{2\Delta r} + \mathcal{O}(\Delta r^2)u'' , \\ \left( \frac{\partial^2}{\partial r^2} u \right)_{j>0} &= \frac{u_{j+1} + u_{j-1} - 2u_j}{(\Delta r)^2} + \mathcal{O}(\Delta r)u''' . \end{aligned} \quad (3.16)$$

In polar coordinates, the above equations do not hold for  $j = 0$ , because  $u_j$  is only defined for non-negative values of  $j$ . The radial symmetry implies  $u_j = u_{-j}$ , hence the first order derivative vanishes at  $j = 0$ , which is also supported by the fact that a realistic electric field is only given if the function is steady on axis at  $r = 0$ .

$$\begin{aligned} \left( \frac{\partial}{\partial r} u \right)_{j=0} &= 0 , \\ \left( \frac{\partial^2}{\partial r^2} u \right)_{j=0} &= \frac{2(u_1 - u_0)}{(\Delta r)^2} . \end{aligned} \quad (3.17)$$

For the Laplacian, the first derivative additionally has to be divided by  $r$ , yielding a singularity on axis. An examination of the limit  $r \rightarrow 0$  resolves this problem using l'Hospital's rule:

$$\lim_{r \rightarrow 0} \frac{u'(r)}{r} \stackrel{l'H}{=} \lim_{r \rightarrow 0} \frac{u''(r)}{1} = u''(0) = \frac{2(u_1 - u_0)}{(\Delta r)^2} . \quad (3.18)$$

With these necessary preparations the discretized Laplacian for a polar geometry can be written as:

$$\begin{aligned}
 (\nabla_{\perp}^2 u)_{j=0} &= \frac{4(u_1 - u_0)}{(\Delta r)^2} , \\
 (\nabla_{\perp}^2 u)_{j>0} &= \frac{\left(1 + \frac{1}{2j}\right) u_{j+1} + \left(1 - \frac{1}{2j}\right) u_{j-1} - 2u_j}{(\Delta r)^2} .
 \end{aligned} \tag{3.19}$$

Now, the propagation equation (3.12) can be rewritten in a discretized form. Using a *Crank-Nicholson* (CN) differencing scheme, one obtains,

$$\left[1 - \frac{1}{2} (D\Delta z) \nabla_{\perp}^2\right] u^{n+1} = \left[1 + \frac{1}{2} (D\Delta z) \nabla_{\perp}^2\right] u^n - \frac{1}{2} (D\Delta z) S^n . \tag{3.20}$$

This scheme compares the old solution of the partial differential equation  $u^n$  with the new solution  $u^{n+1}$  at a point  $(n+1/2)\Delta z$  along the propagation axis, resulting in second order accuracy in  $z$  [18]. Equation (3.20) can be written as a matrix equation,

$$\mathcal{A}u^{n+1} = b(u^n, S^n) = b^n , \tag{3.21}$$

with a tridiagonal, easily invertible matrix  $\mathcal{A}$ . Standard methods of computation allow for a solution of the system within the order of  $\mathcal{O}(N)$  operations [18].

The source terms  $S_{1/q_j}^n$  for the laser and the harmonic field, respectively were introduced in equations (2.36) and (2.38), in atomic units and according to the notation in this chapter they read as

$$S_{1j}^n(\omega_k) = \frac{4\pi}{c^2} n_0 \hat{F}^+ [ \{1 - R(r_j, z_n, t)\} E_1(r_j, z_n, t) ]_{\omega=\omega_k} , \tag{3.22}$$

$$S_{qj}^n(\omega_k) = -\mu_0 n_0 \omega_k^2 \hat{F}^+ [ R^2(r_j, z_n, t) x(r_j, z_n, t) ]_{\omega=\omega_k} . \tag{3.23}$$

$\hat{F}^+$  denotes the Fourier transform operator for a transform from time to frequency domain. All variables in the above equation are in atomic units.

### 3.3.2 Stability Analysis

A very important property of a differencing scheme is its stability. In textbooks, e.g. [18], unconditional stability is proposed for the CN scheme. Unfortunately,

this is not completely true for a radial symmetric grid due to the  $(1/r)$ -term in the Laplacian. To study the stability of the differencing scheme given in eq. (3.20), a *von Neumann stability analysis* was performed (see appendix C). The von Neumann analysis is a local method, where the coefficients of the differencing equations are considered as constant in  $r$ - and  $z$ -space. In that case the independent solutions of the partial differential equation under neglect of the source term can be written in terms of transverse eigenmodes of the form

$$v_j^n(k) = \xi^n(k) e^{ikj\Delta r} , \quad (3.24)$$

for any real wavenumber  $k$  in the transverse direction and with  $\xi^n(k)$  denoting the amplitude of the corresponding eigenmode after the  $n$ -th iteration step. In a next step, these eigenmodes are supplied to the differencing scheme without the source term, which is then solved for the amplification factor

$$g(k) = \frac{\xi^{n+1}}{\xi^n} . \quad (3.25)$$

The differencing scheme is stable for those eigenmodes  $v_j^n(k)$ , where

$$|g(k)|^2 \leq 1 . \quad (3.26)$$

For the underlying scheme, eq. (3.20), the above constraint leads to a correlation between the stable wavenumbers  $k$  and the radial discretization  $\Delta r$ :

$$\begin{aligned} |g|^2 &= \frac{(1 + \frac{\alpha}{j} \sin(k\Delta r))^2 + 4(\alpha [\cos(k\Delta r) - 1])^2}{(1 - \frac{\alpha}{j} \sin(k\Delta r))^2 + 4(\alpha [\cos(k\Delta r) - 1])^2} \leq 1 , \\ \implies \alpha \sin(k\Delta r) &\leq -\alpha \sin(k\Delta r) . \end{aligned} \quad (3.27)$$

With  $\alpha = c\Delta z/\omega(\Delta r)^2 > 0$ , the final stability criterion reads as:

$$\begin{aligned} \sin(k\Delta r) &\leq 0 , \\ \implies (2n - 1)\pi &\leq k\Delta r \leq 2n\pi , \quad n \in \mathbb{Z} . \end{aligned} \quad (3.28)$$

Like the 'normal' CN-scheme, the radial symmetric scheme is unconditionally stable for any stepsize  $\Delta z$ . However, to obtain reasonable results on a local scale,  $\Delta z$  should be in the range of the wavelength  $\lambda$ , which defines the characteristic scale of variation of the fields. Applying large stepsizes up to infinity would

asymptotically result in the equilibrium solution of the system.

But, the stability criterion does limit the gridwidth  $\Delta r$ . Transferring eq. (3.28) to terms of wavelengths ( $k = 2\pi/\lambda$ ) and setting  $n = 1$ , wavelengths which fulfill the condition

$$\Delta r \leq \lambda_1 \leq 2\Delta r \quad (3.29)$$

are integrated stable.

Additionally, due to the periodicity of the restriction in (3.28), all odd multiples of  $k$  and therefore all  $\lambda_q = \lambda_1/q$ ,  $q \in (2\mathbb{N}_0 + 1)$  are stable. Fortunately, these are just the wavelengths produced by the HHG process, so that once a value for  $\Delta r$  is found, which gives a stable scheme for the fundamental laser wavelength, all produced harmonics are integrated stable as well. Thus only numerical noise will be amplified in the unstable regions. As a solution for simulations, where not only the odd harmonics have to be propagated, one might use several radial grids, so that there is a stable band for every concerned wavelength.

The most intuitive choice of  $\Delta r$  is such, that the fundamental wavelength  $\lambda_1$  lies in the middle of the first stable band:

$$\Delta r = \frac{2}{3}\lambda_1 . \quad (3.30)$$

### 3.4 Simulation Sequence

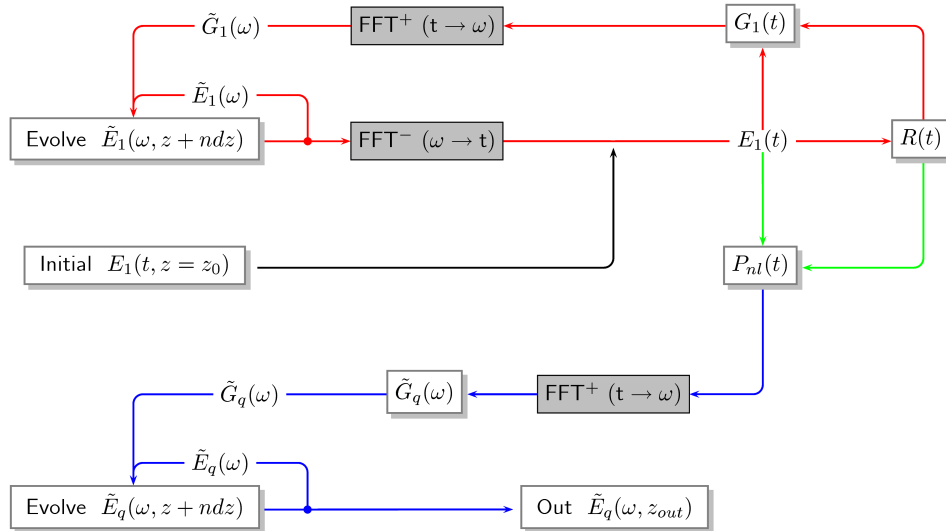


Figure 3.1: Flowchart of the HHG simulation code  $\mathcal{R}$ HYNO

The flowchart in figure 3.1 illustrates the flow of the simulation data through the individual functions.

At first initialization proceeds, i.e. a parameter file and all given command-line options are evaluated. Default values are assumed for those parameters which have been left undefined to prevent an abnormal termination of the program. Table 3.4 shows a list of all input parameters, their defaults and a short description.

Next, the fundamental radiation  $E_1(r, z_0, t)$  is initialized as a gaussian beam in space and time with pulse duration  $\tau$  (FWHM), waist  $W_0$ , the position of the focal spot relative to the beginning of the interaction region  $z_f$ , carrier frequency  $\omega_0$  and an initial peak intensity of the electro-magnetic field  $I_0$ :

$$\begin{aligned} E_1(r, z_0, t) &= E_1(r, -z_f, t) \\ &= E_0 \frac{q_0}{q_{-z_f}} \exp \left[ -\frac{i\omega_0}{c} \left( \frac{r^2}{2q_{-z_f}} - z_f - ct \right) - 4 \ln(2) \left( \frac{t}{\tau} \right)^2 \right], \end{aligned} \quad (3.31)$$

with

$$E_0 = \sqrt{I_0/\epsilon_0 c}, \quad q_0 = i \frac{\omega_0 W_0^2}{2c}, \quad q_{-z_f} = -z_f + q_0.$$

The harmonic field is initialized with zeros.

After initialization, the main simulation loop starts with the calculation of the probability for an atom to be ionized, see eq. (2.5),

$$R(t) = \exp \left[ - \int_{-t_0}^t w(t') dt' \right], \quad (3.32)$$

with the ADK rate  $w(t')$ , eq. (2.3). The integration starts at  $t_0$  instead of  $-\infty$  because only a finite interval contributes to the integral. However, as the fundamental laser field was initialized such, that it vanishes at the lower border of the simulated time window  $T$ , equation (3.32) still gives reliable results within these new borders.

Now, the core of the simulation, the non-linear, laser-induced single atom dipole moment  $x(t)$ , eq. (3.6), will be computed. The integral over the time of flight  $\tau$  is performed for every point in time  $t_k$  of the temporal grid. Because of the prefactor proportional to  $\tau^{-3/2}$  in the integrand, contributions to the HHG process from electrons which have not returned to the nucleus after the first

Parameter	Default value	Unit	Description
$N_{steps}$	10	-	Propagation steps between source evaluations
$N_{runs}$	10	-	Number of source evaluations between data output
$N_{pics}$	1	-	Number of data outputs
$N_{oc}$	3	-	Number of optical cycles to take into account for the calculation of the induced dipole moment
$\lambda_1$	$740 \times 10^{-9}$	$m$	Wavelength of the fundamental laser beam
$\tau$	$30 \times 10^{-15}$	$fs$	Duration of the laser pulse defined as FWHM
$W_0$	$25 \times 10^{-6}$	$m$	Waist of the laser at its focal spot
$z_f$	0	$m$	Position of the focal spot relative to the beginning of the interaction region
$I_0$	$8 \times 10^{14}$	$W/cm^2$	Peak intensity of the laser in the focal spot
$N_r$	101	-	Number of radial (spatial) grid points
$\Delta r$	$2\lambda_1/3$	$m$	Radial grid width
$r_{max}$	$(N_r - 1) * \Delta r$	$m$	Max. radius of the spatial grid
$\Delta z$	$10^{-6}$	$m$	Propagation stepsize
$Z$	0.99560	-	Resulting net charge of the ionic core (default: Neon, value taken from [16])
$I_p$	21.6	$eV$	Ionization potential (default: Neon)
$p_0$	50	$mbar$	Gas pressure
$T$	293	$K$	Gas temperature
$Q$	300	-	Max. sampled frequency in units of $\omega_0$
$L$	3	-	Min. size of the time window in units of the pulse duration $\tau$ (FWHM)
$N_t$	16384	-	Number of points in $\omega$ - and $t$ -space
$I_{min}$	$10^{12}$	$W/cm^2$	Min. peak intensity (threshold) to start the calculation of a single atom spectrum

Table 3.1: *Input parameters of the HHG simulation tool RHYNO*

few cycles can be neglected. Hence, in order to increase computation speed, the integral is evaluated only over a few optical cycles of the laser. The number of cycles the integration takes into account can be adjusted in the simulation code with the parameter  $N_{oc}$ . Its default value is  $N_{oc} = 3$ .

Another parameter, which was introduced into the code to shorten calculation time is the threshold intensity  $I_{min}$ . It defines the minimal peak intensity the fundamental must have at a certain point  $r_j$  in order to start the calculation of the non-linear dipole moment. HHG is a strong-field process and will not occur for intensities much smaller than  $10^{14} \text{ W/cm}^2$ . Since a study of the behaviour of the HHG signal under variation of the threshold intensity was not in the scope of this work, its default value is set to  $I_{min} = 10^{12} \text{ W/cm}^2$ , to ensure reliable results. The dipole moment is set equal to zero for any  $r_j$ , where the minimum peak intensity is not achieved.

After calculation of the probability for an atom to be unionized  $R(t)$  and the induced dipole moment  $x(t)$  for every  $r_j$ , the source terms can be constructed. The fundamental source is built within the time domain and Fourier transformed as described by eq. (3.22).

To set up the harmonic source, the non-linear polarization  $P_{nl}$ , eq.(2.39), is constructed and Fourier transformed. Then, every frequency slice  $k$  of the transform is multiplied by its squared frequency  $\omega_k^2$  and a prefactor in order to obtain the non-linear source term as defined in (3.23).

Finally the propagation routine is started for both, the laser and the XUV-light. The propagation equation is solved  $N_{steps}$  times to evolve the fields to  $z' = z + N_{steps} \Delta z$ . The parameter  $N_{steps}$  defines the number of propagation steps until the next evaluation of the sources. Due to the fact that the peak amplitude of the fundamental is slowly varying along the propagation axis, it is not necessary to recalculate the sources after every propagation step, thus saving an enormous amount of calculation time. The code uses  $N_{steps} = 10$  as default value.

After the fields have been evolved, the fundamental laser field is Fourier transformed back to time domain and the simulation loop is restarted.

The simulation data might be saved each time after propagation. In order to control the number and time of data outputs, two additional parameters were introduced into the program,  $N_{pics}$  and  $N_{runs}$ . The number of source evaluations until the data is saved is defined by  $N_{runs}$ , whereas  $N_{pics}$  defines the number of snapshots of the fields which are taken during the simulation. Thus a snapshot is taken every  $N_{runs} * N_{steps}$  propagation steps at  $z = z_0 + N_{runs} N_{steps} \Delta z$ . Hence, the  $n_p$ th picture corresponds to

$$z_{n_p} = z_0 + n_p N_{runs} N_{pics} \Delta z \quad (3.33)$$

and the total length of the simulated gas medium is given by

$$z_{tot} = z_0 + N_{pics} N_{runs} N_{steps} \Delta z . \quad (3.34)$$



---

# 4

## HHG Simulation Results

---

Using the code  $\mathcal{R}\text{HYNO}$ , the characteristics of the HHG radiation were investigated. The results of these simulations are presented in this chapter. The first section elaborates on the cut-off rule. A comparison of the estimated cut-off frequency and the cut-off seen in the simulated spectra is given. In the second section, the behavior of the HHG spectra under variation of the laser pulse duration is investigated. The dependence of the linewidth on the duration of the generating pulse is discussed. The position of the laser focus relative to the gas medium has a crucial influence on the HHG spectra. The reason is the different phase of the fundamental radiation for a different focal position. To ensure higher power at a particular harmonic, the phase, i.e. the position of the focus, has to be optimized. Simulation results for this so-called phase matching are shown in the last section of the chapter.

### 4.1 Cut-off Law

One of the main characteristics of the HHG process is the cut-off frequency in the spectra. According to the Simple Man Model, section 2.1, an approximate cut-off law is given by eq. (2.11) from which the maximum harmonic number can be estimated as

$$q_c = \frac{I_p + 3.17 U_p}{\hbar\omega_0} . \quad (4.1)$$

Table 4.1 shows selected peak intensities of the fundamental laser and the corresponding maximum harmonic number (estimated and simulated) for the case of a Neon gas target ( $I_p = 21.6 \text{ eV}$ ). The HHG spectra are shown in figure 4.1. The fundamental laser was initialized with a pulse duration of  $\tau = 20 \text{ fs}$  and a waist of  $W_0 = 17.6 \text{ }\mu\text{m}$ . The power spectra were calculated in the focus of the laser.

Peak Intensity $I_0$ [ $\text{W}/\text{cm}^2$ ]	Estimated Cut-off	Simulated Cut-off
$1 * 10^{14}$	17.7	21 – 25
$5 * 10^{14}$	37.1	39 – 43
$1 * 10^{15}$	61.3	63 – 67

Table 4.1: *Maximum harmonic numbers estimated from the cut-off law and simulation for selected peak intensities of the fundamental laser beam and a Neon gas target ( $I_p = 21.6 \text{ eV}$ ).*

As expected from theoretical considerations [4], the classical cut-off law gives a better approximation for higher intensities. The reason is that the ratio of the ponderomotive potential  $U_p$  and the ionization potential  $I_p$  increases.

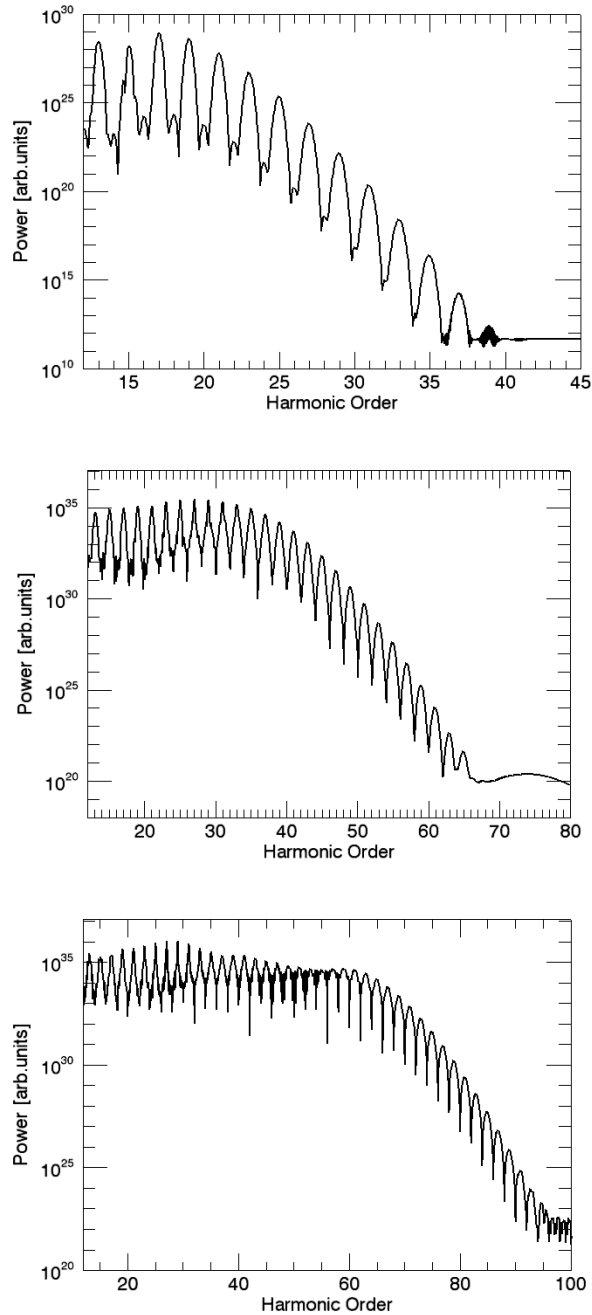


Figure 4.1: *Logarithmic scaled power spectra to show the cut-off for peak intensities of  $10^{14} \text{ W/cm}^2$  (top),  $5 \cdot 10^{14} \text{ W/cm}^2$  (middle) and  $10^{15} \text{ W/cm}^2$  (bottom).*

## 4.2 Influence of the Laser Pulse Length

The influence of the pulse duration  $\tau$  on the HHG spectra was investigated for the present work. The spectra in figures 4.2, 4.3 and 4.4. show simulations for different pulse durations, i.e. 7 fs, 15 fs, 20 fs and 30 fs. To calculate these spectra, a laser focus at the beginning of the gas medium and a waist of  $W_0 = 17.6 \mu m$  were assumed.

For a first set of simulations, the peak intensity was kept constant at  $7.5 * 10^{14} W/cm^2$  for the different pulse durations. Thus the total energies of the laser pulse  $E$  varied with the pulse length (figs. 4.2, 4.3). The total energies are given in the captions of the figures.

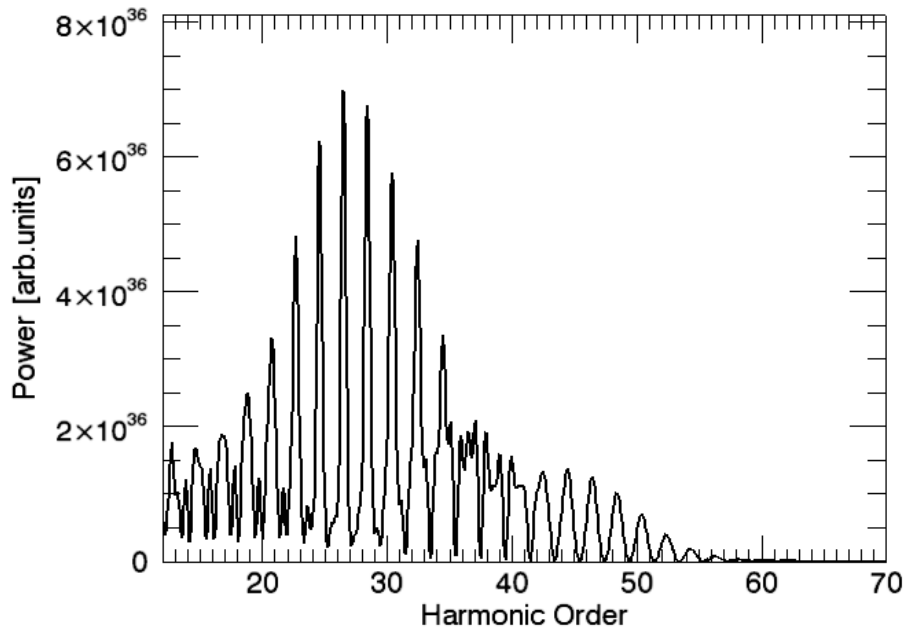
The linewidths of the harmonics are narrower for longer pulses. This is due to the Fourier limit on the bandwidth of the pulses, which states that shorter pulses have a broader spectrum, thus a broader band of frequencies stimulates the HHG process. Another interesting result is that the harmonics are no longer only odd multiples of the fundamental for very short pulses. This agrees with the theoretical prediction (see section 2.1), where the presence of only odd harmonics is linked to a large number of optical cycles of the fundamental contributing to HHG.

For the second set of simulations, the total pulse energy was held constant at  $E = 0.57 mJ$ . Therefore the peak intensities changed for different pulse durations, their values are given in the captions of the figures. The change of intensity causes the dominant effect of the frequency cut-off as visualized in figure 4.4 for a 7 fs and a 30 fs pulse. (The other spectra are shown in appendix D.) However, their linewidths still change as expected.

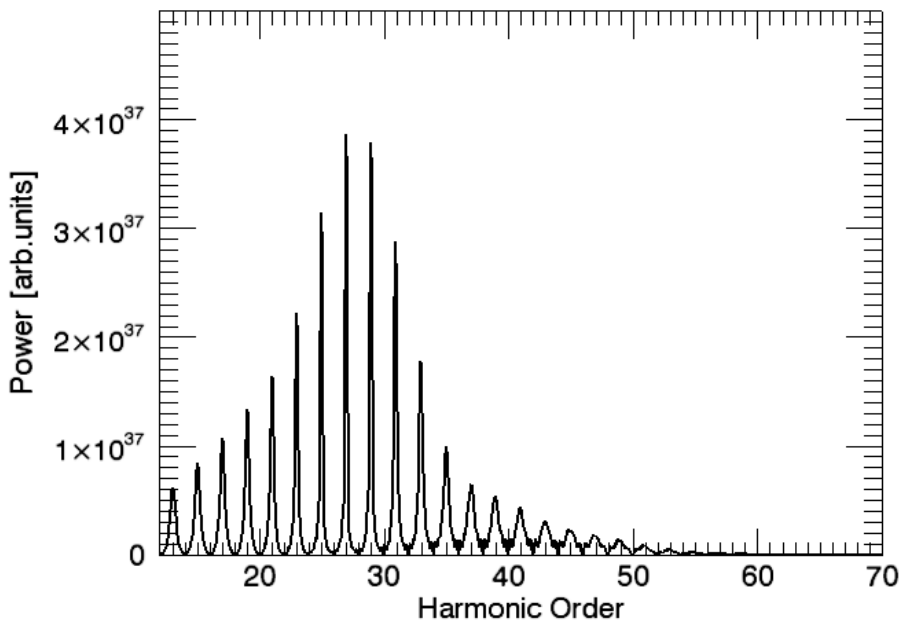
## 4.3 Phase Matching

The strong dependance of the HHG spectra on the phase of the fundamental laser was investigated by varying the position of the focus relative to the beginning of the gas medium.

Figure 4.5 shows HHG spectra for three different focal positions resulting from simulations of a laser pulse with the wavelength  $\lambda = 740 nm$ , pulse duration  $\tau = 7 fs$ , waist size  $W_0 = 17.6 \mu m$  and a peak intensity at the beginning of the interaction region of  $3.95 * 10^{14} W/cm^2$ . For these simulations a HHG setup with a 0.6 mm long, Neon gas filled cell was assumed. The pictures illustrate the strong dependance of the spectra on the position of the focus and imply, that there is an optimal value for the position of the focal spot  $z_f$  to generate a maximum output for a desired harmonic. As the position of the focus is linked to the phase of the radiation in the interaction region, this dependancy is called phase-matching, see eq. (2.13).

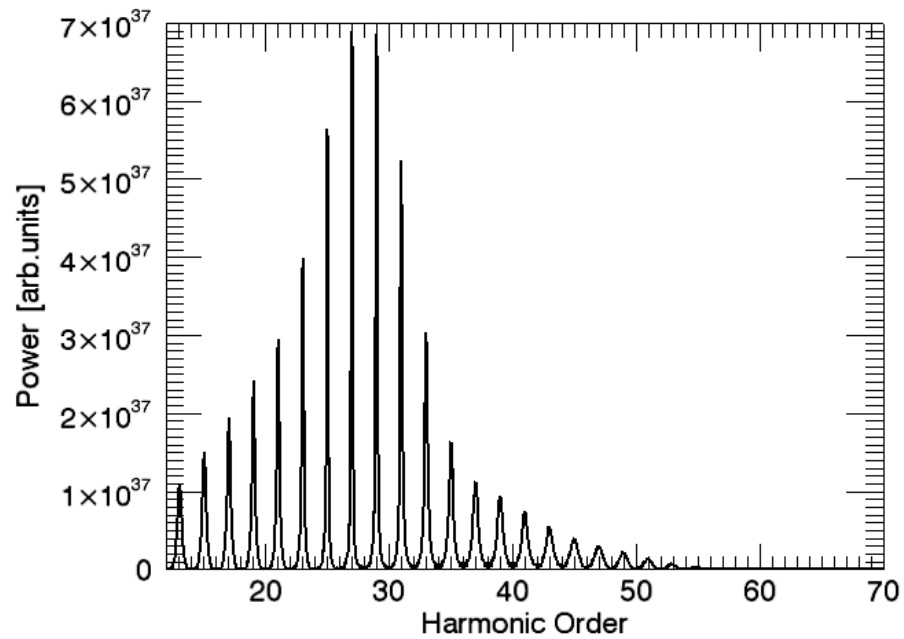


$\tau = 7 \text{ fs}, E = 0.43 \text{ mJ}$

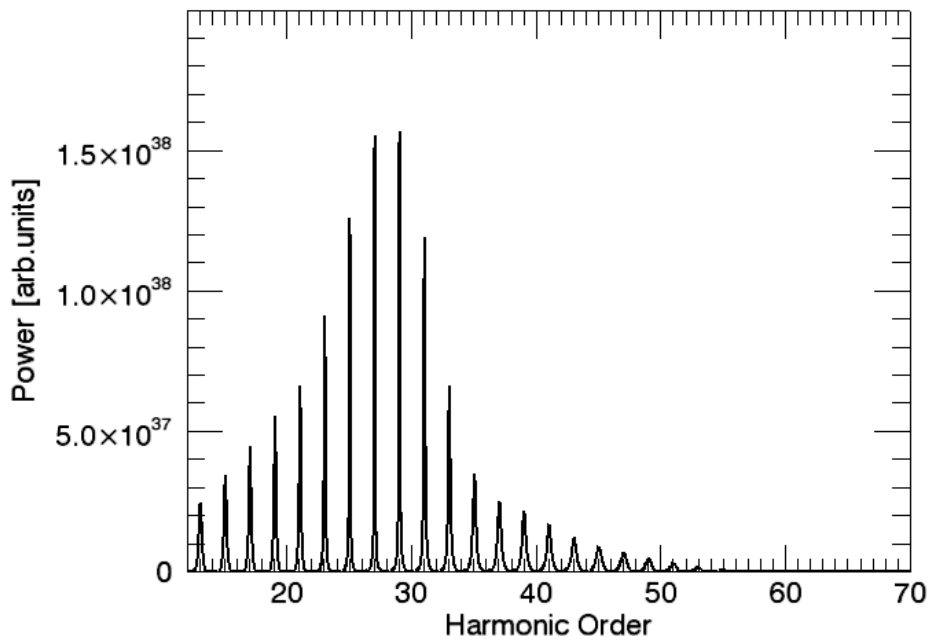


$\tau = 15 \text{ fs}, E = 0.91 \text{ mJ}$

Figure 4.2: *HHG power spectra for different pulse durations with a constant peak intensity of the fundamental laser  $I_0 = 7.5 * 10^{14} \text{ W/cm}^2$ .*

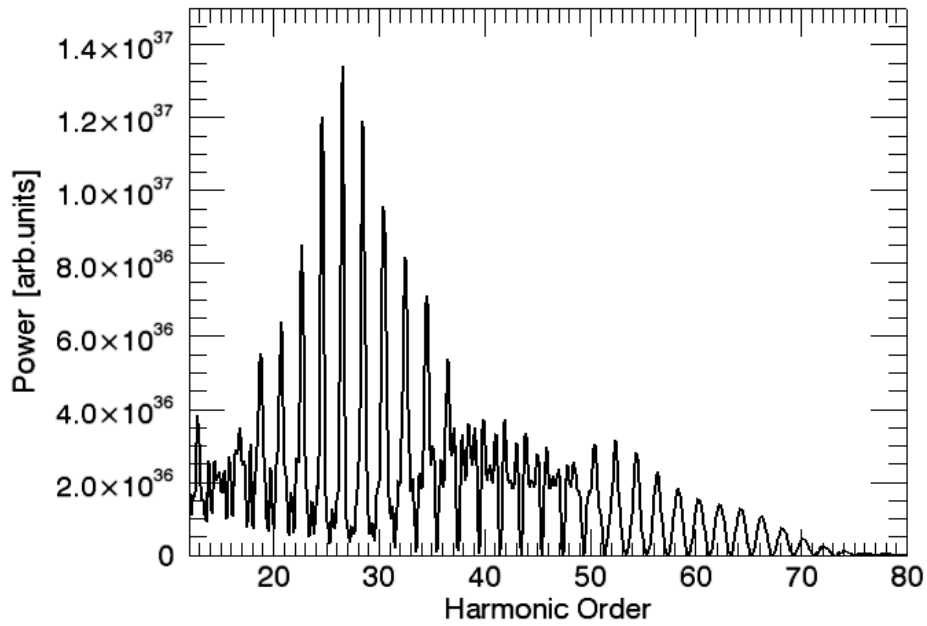


$\tau = 20$  fs,  $E = 1.22$  mJ

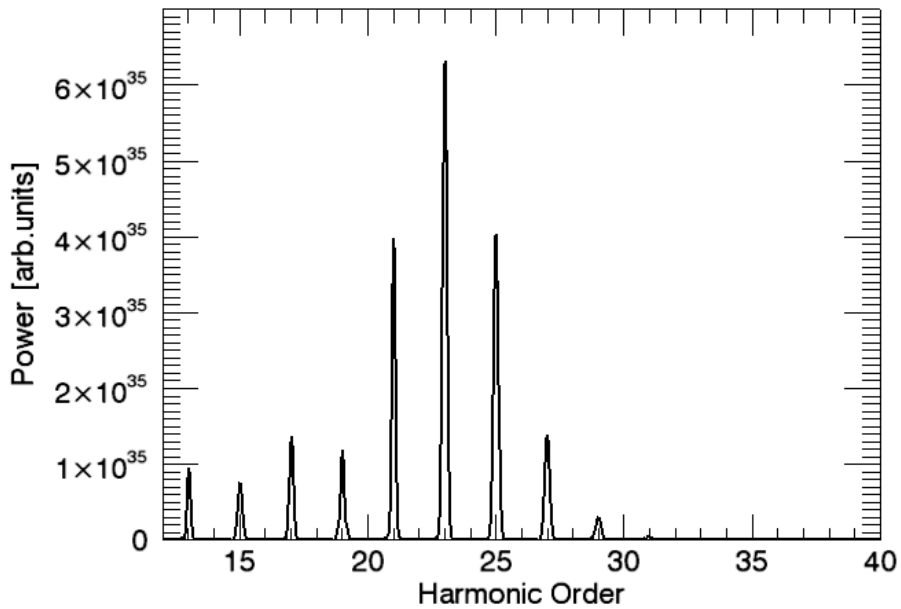


$\tau = 30$  fs,  $E = 1.83$  mJ

Figure 4.3: *HHG power spectra for different pulse durations with a constant peak intensity of the fundamental laser  $I_0 = 7.5 \times 10^{14}$  W/cm<sup>2</sup>.*



$$\tau = 7 \text{ fs}, I_0 = 1 * 10^{15} \text{ W/cm}^2$$



$$\tau = 30 \text{ fs}, I_0 = 2.3 * 10^{14} \text{ W/cm}^2$$

Figure 4.4: *HHG power spectra for different pulse durations and peak intensities with a constant total pulse energy of the fundamental laser  $E = 0.57 \text{ mJ}$ .*

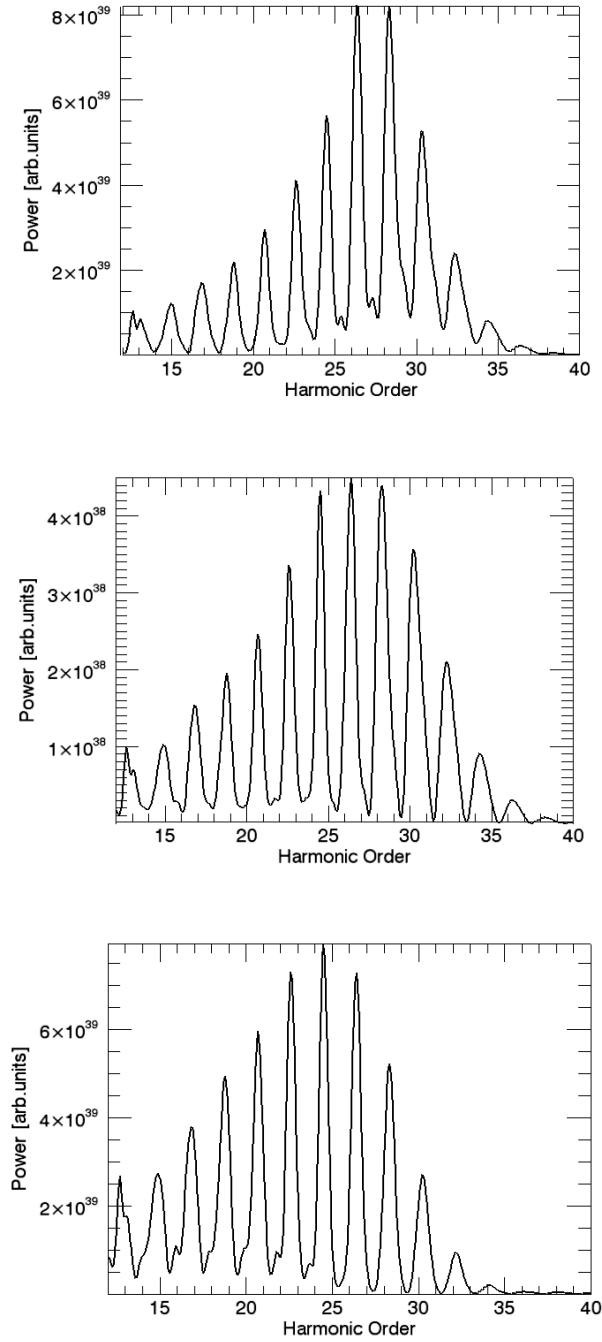


Figure 4.5: Macroscopic HHG power spectra for different positions of the laser focus  $z_f$  relative to the beginning of a 0.6 mm long gas-cell:  $z_f = -1.5$  mm (top),  $z_f = 0$  mm (middle) and  $z_f = +1.5$  mm (bottom). The spectra were calculated for a stimulating laser pulse with a duration of  $\tau = 7$  fs and peak intensity of  $I_0 = 3.95 \times 10^{14}$  W/cm<sup>2</sup> at the beginning of the interaction region.



---

# 5

## FEL Simulations with Genesis 1.3

---

To investigate the use of the HHG radiation as a suitable seed for seeded FEL projects, two examples have been elaborated: The final amplifier of the Low-Energy (LE) BESSY-FEL and the second radiator of STARS [1, 19]. These FELs were proposed to be based on the seeded High Gain Harmonic Generation (HG) principle, where the frequency of the radiation is up-converted in several HG stages. In such a cascaded multi-stage HG-FEL, the radiation output quality suffers with an increasing number of stages due to the accumulation of sidebands and the loss of electron beam quality [1]. Therefore it is desirable to shorten the setup, by using a seed close to or even in the output range of the FEL. The HHG process delivers these short wavelengths in the nanometer range. Frequency filtering effects during the FEL process make it possible to use the full, unfiltered HHG radiation as a seed source [12, 13, 14]. Therefore FEL simulations were performed supplying the simulated HHG spectra from  $\mathcal{R}HYNO$  as seeding radiation to the 3D FEL code GENESIS 1.3 [5].

The first section shows the simulated HHG radiation, which was supplied as a seed to the FEL process, whereas the results of the FEL simulation cases are presented in sections 2 and 3.

### 5.1 The HHG Seed

The resonant wavelength of the FEL setup was tuned to  $23.9 \text{ nm}$  for the Low-Energy FEL and  $32.2 \text{ nm}$  for STARS corresponding to the 31st or the 23rd harmonic of the fundamental laser beam, respectively. To enhance the contribution of these harmonics, HHG radiation originating from a  $30 \text{ fs}$  laser pulse at a wavelength of  $740 \text{ nm}$  focused to a point  $1.5 \text{ mm}$  before a Neon filled gas cell was assumed. The intensity of the laser was about  $3.5 * 10^{14} \text{ W/cm}^2$  at the beginning of the interaction region, see figure 5.1.

However, with respect to Nyquist's sampling theorem [18], the simulated spectra have to be filtered in order to match the sampling range of GENESIS 1.3. The spectra were therefore reduced to contain only wavelengths  $\lambda \in [\frac{1}{2} \lambda_r; \frac{3}{2} \lambda_r]$ , with  $\lambda_r$  denoting the resonant wavelength of the FEL [12]. Note that this sort of frequency filtering is only necessary due to numerical restrictions and is not needed for a real experiment.

The calculated spectra were transformed to GENESIS 1.3 conform input data,

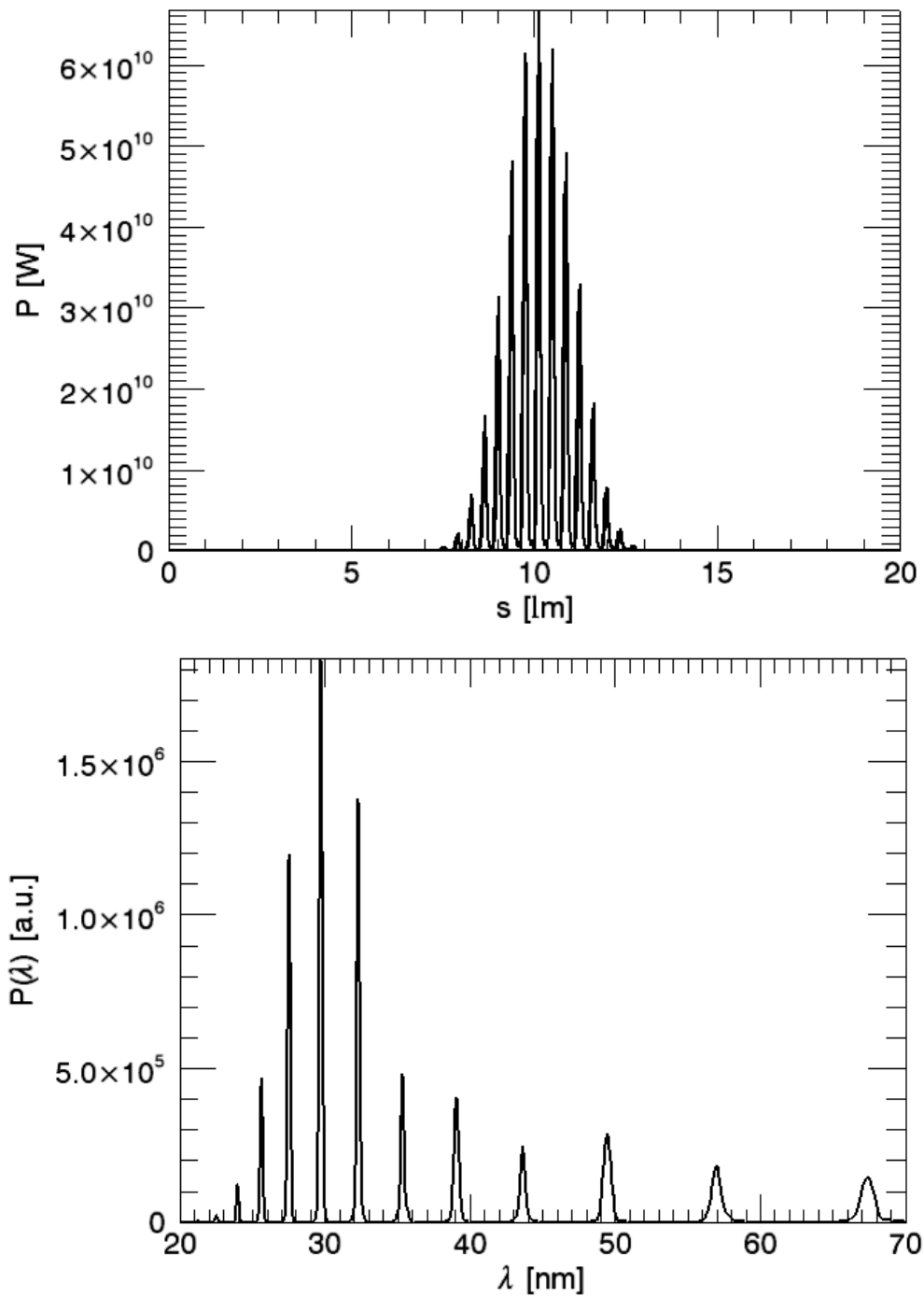


Figure 5.1: *Time resolved (top) and spectral (bottom) power distribution of the unfiltered HHG seed.*

using its dfl-file option for three-dimensional input of seeding radiation. Because reliable absolute values for the intensity of the HHG radiation are not obtainable from the SFA, the spectra were normalized to be in an output range as experimentally observed (i.e. a conversion factor of  $10^{-5}$  was used [20]).

To take into account the loss of intensity during transportation of the seeding radiation to the FEL device, further seeds with reduced intensity were prepared for GENESIS 1.3 runs.

## 5.2 STARS

STARS is designed to serve as a demonstrator on seeded HHG FELs with a two stage configuration. The radiator of the second stage will be tuneable to directly lase at wavelengths in the range of 40 *nm* to 70 *nm* [19]. However, using the third harmonic content of the FEL radiation, wavelengths down to 13 *nm* will be accessible for experiments [21].

For this study, the second radiator of STARS was tuned to lase at 32.2 *nm*, corresponding to the 23rd harmonic of the laser beam. For the simulation a 325 *MeV* electron beam with a peak current of  $I_{\text{peak}} = 500 \text{ A}$  and a relative energy spread of  $3 * 10^{-5}$  was assumed. The second radiator will consist of  $3 * 150$  periods with a length of  $\lambda_u = 22 \text{ mm}$  and two 1 *m* drift sections inbetween, hence it has a total length of roughly 12 *m*. Two seeds with different intensities (figs. 5.2 and 5.3) were prepared for GENESIS 1.3 simulations, as mentioned before.

Figure 5.4 shows how the seeding radiation slips over the electron bunch during the passage through the radiator. Due to the FEL interaction the electrons behind the pulse are prebunched and start to emit radiation at the chosen wavelength. Figures 5.5 and 5.6 show the FEL output at the end of the radiator for two different intensities of the HHG seed. As expected, due to the frequency filtering effect, only the chosen wavelength is amplified inspite of the seeding frequency comb.

An important feature of the BESSY-FEL, as well as of STARS, is the variable polarization of the output radiation. This is possible because the final undulator sections of both FELs are planned as APPLE-III-type helical devices [19]. The HHG radiation is linearly polarized as discussed in chapter 2. However, a pre-bunched electron beam will emit polarized radiation according to the magnetic field configuration of the undulator. Using the first module of the second radiator to imprint an energy modulation with the desired wavelength and thus to produce bunching, the next two APPLE-III-type undulator modules can be used to generate radiation with the selected wavelength and variable polarization. Figure 5.7 shows the results of this simulation for STARS. The temporal and the spectral distribution after 4.25 *m* are depicted.

From these results one can conclude, that seeding STARS with HHG radiation

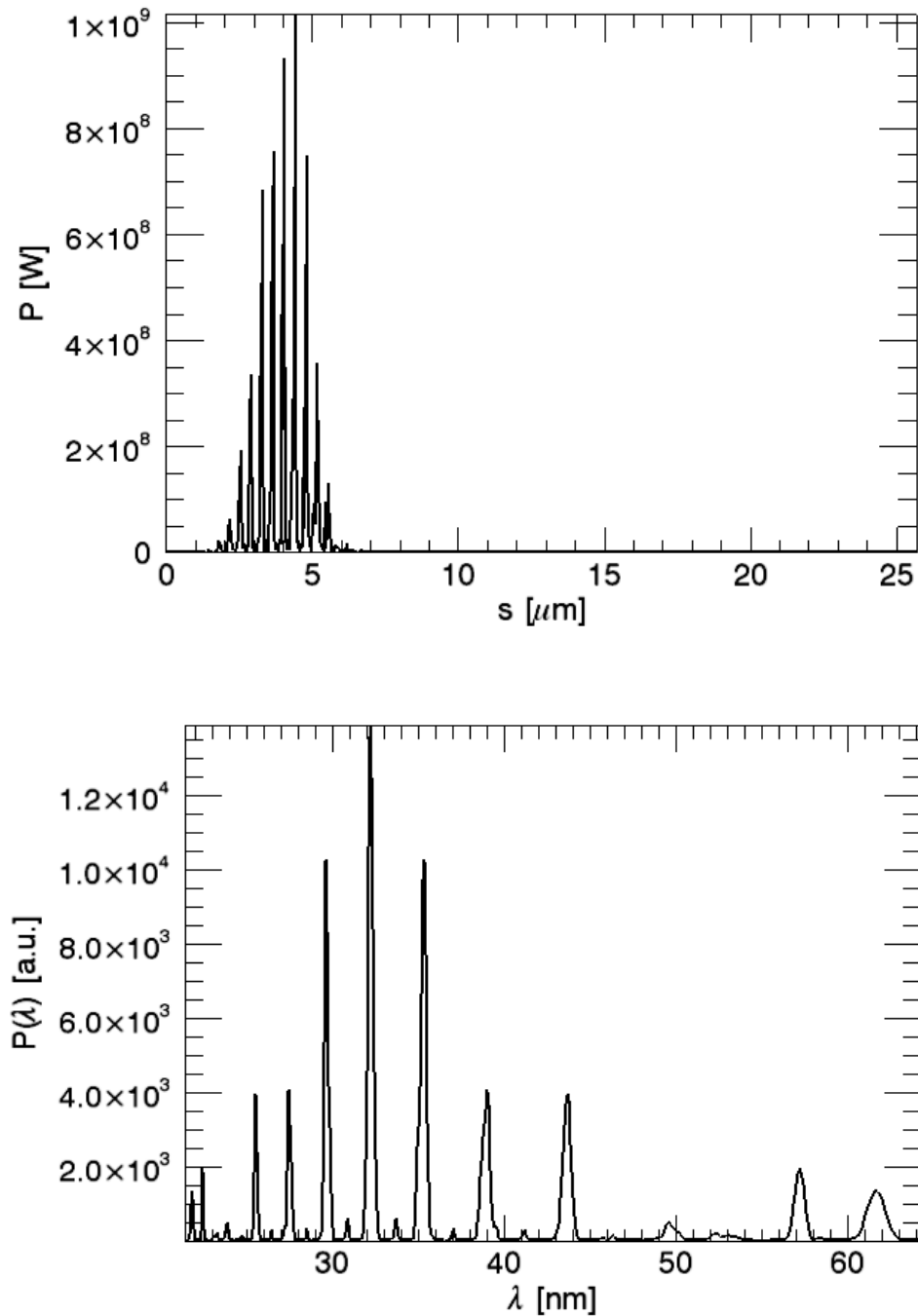


Figure 5.2: Time resolved (top) and spectral (bottom) power distribution of the high intensity HHG seed, filtered and prepared for simulating STARS with GENESIS 1.3.

allows not only for high power and high purity, but also for variable polarization.

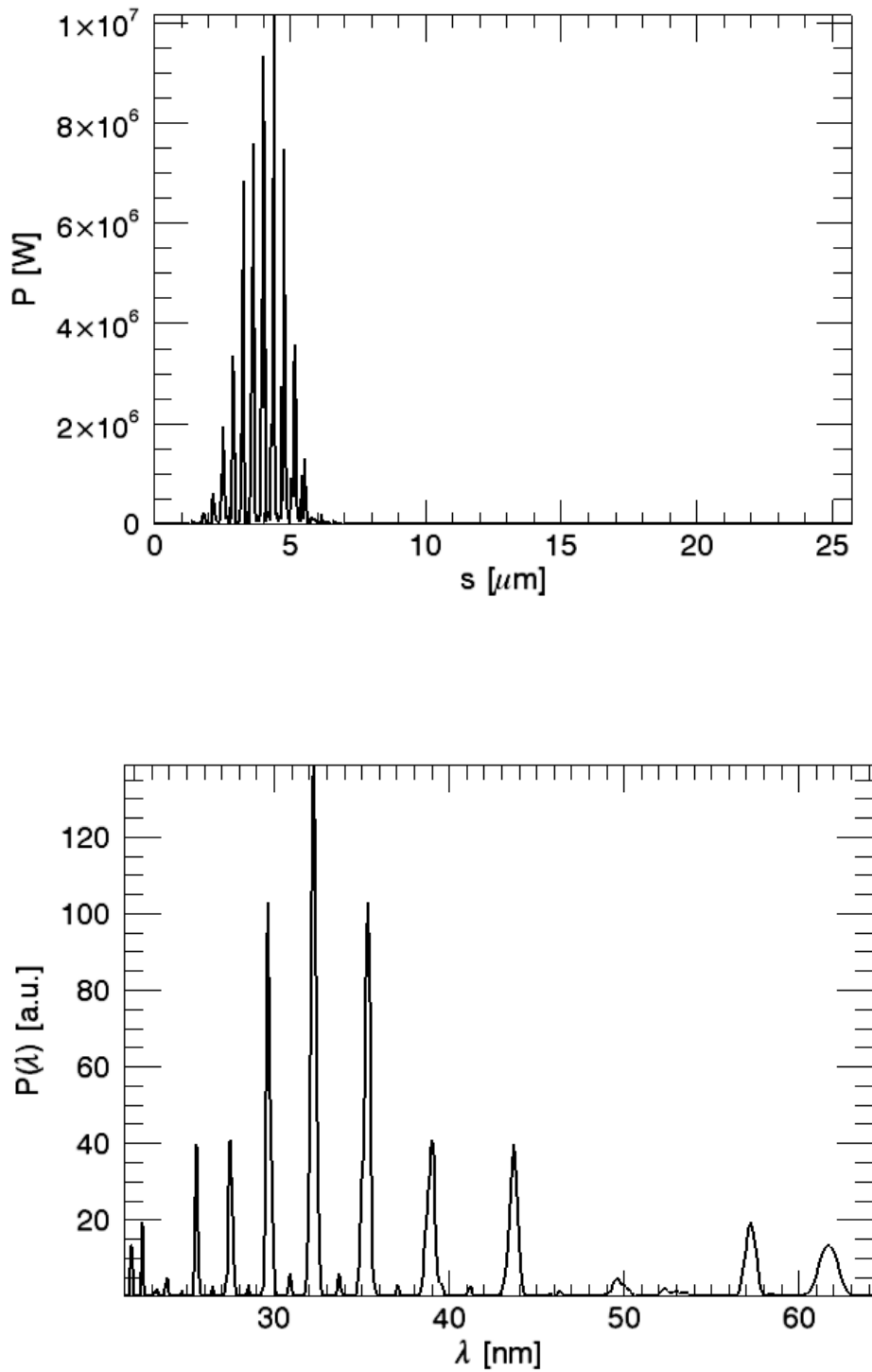


Figure 5.3: *Time resolved (top) and spectral (bottom) power distribution of the low intensity HHG seed, filtered and prepared for simulating STARS with GENESIS 1.3.*

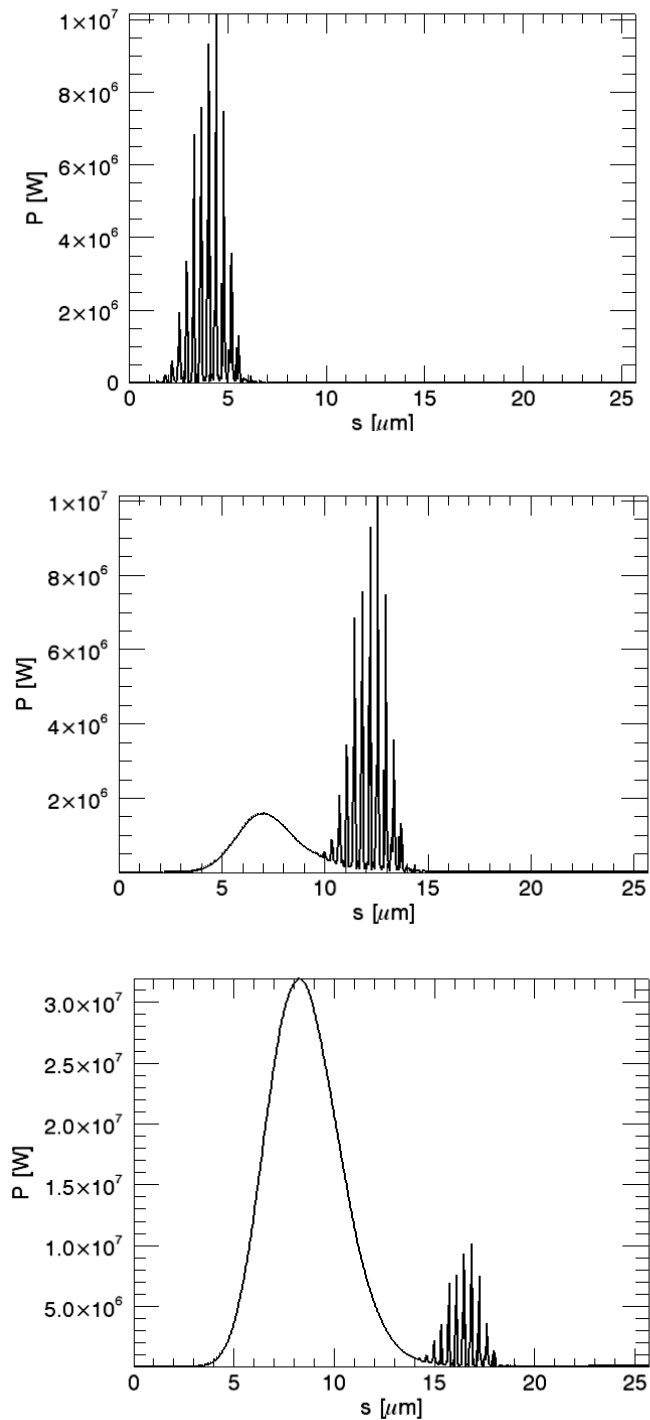


Figure 5.4: Time resolved power distributions to visualize the slippage of the low intensity seeding radiation over the electron bunch inside the final amplifier of STARS. The pictures show the distributions at  $z = 0\text{ m}$  (top),  $z = 5.5\text{ m}$  (middle) and  $z = 8.5\text{ m}$  (bottom) along the propagation axis.

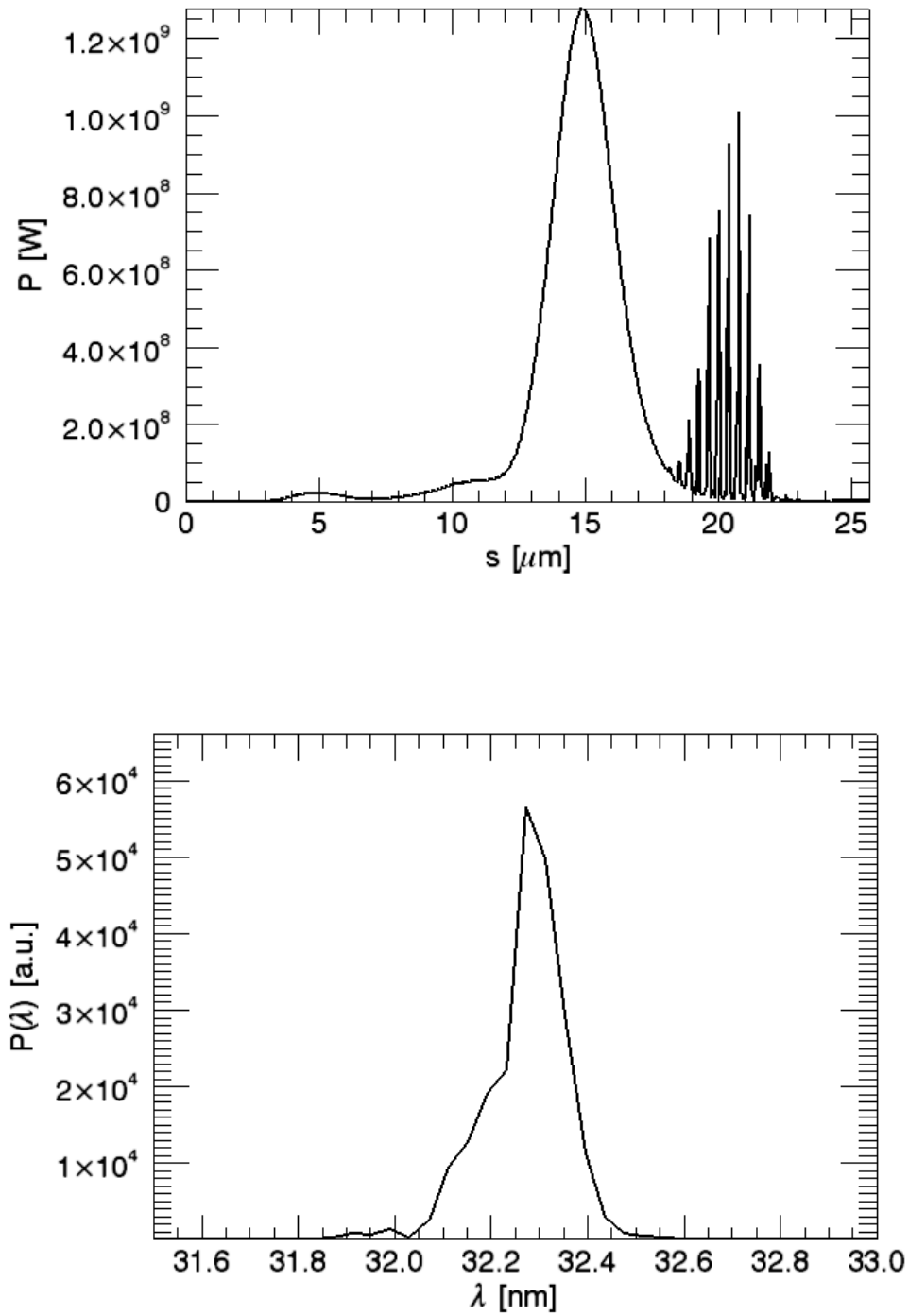


Figure 5.5: *Time resolved (top) and spectral (bottom) power distribution of the simulated FEL output for STARS tuned resonant to  $\lambda = 32.2$  nm and seeded with the low intensity HHG seed.*

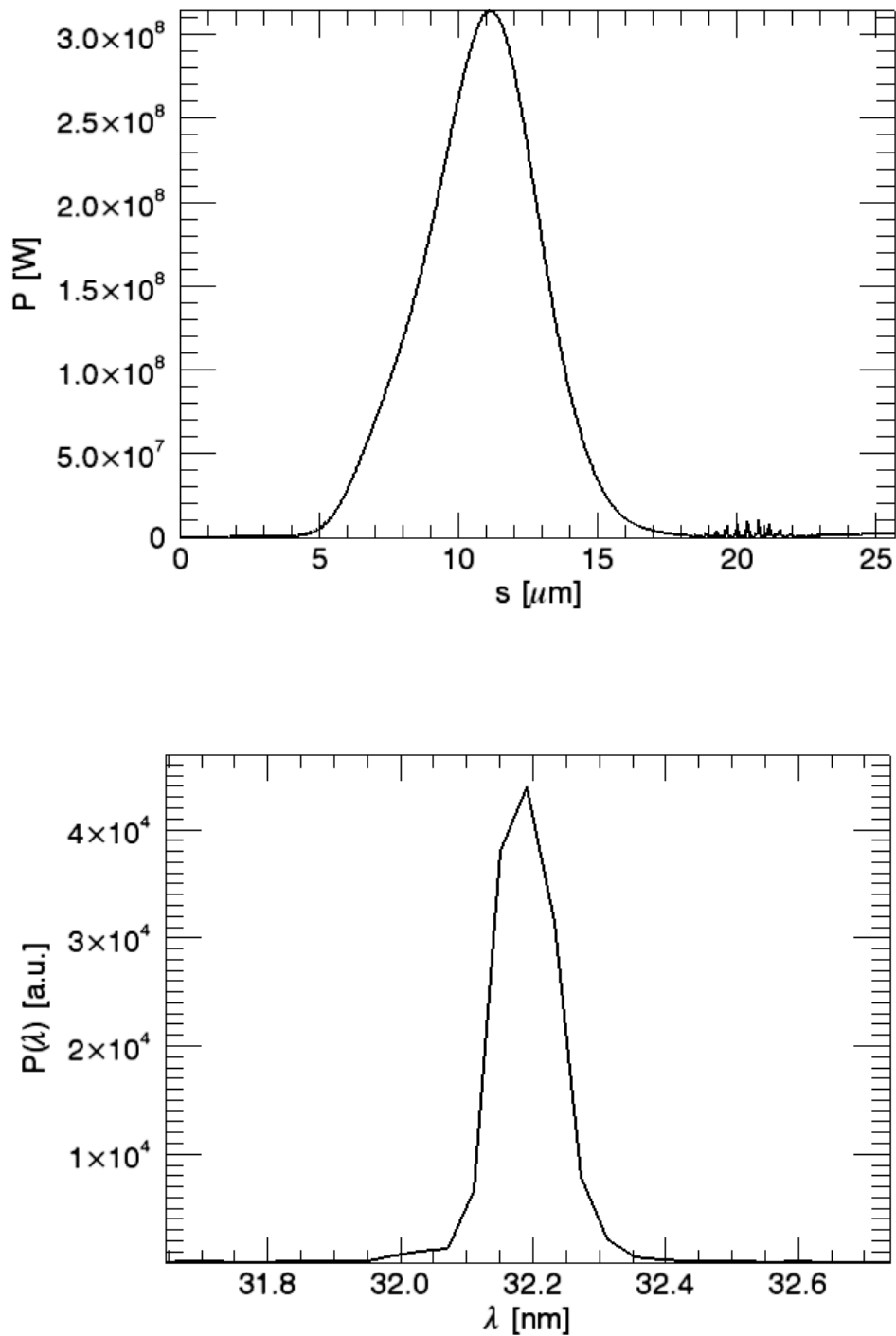


Figure 5.6: *Time resolved (top) and spectral (bottom) power distribution of the simulated FEL output for STARS tuned resonant to  $\lambda = 32.2$  nm and seeded with the high intensity HHG seed.*

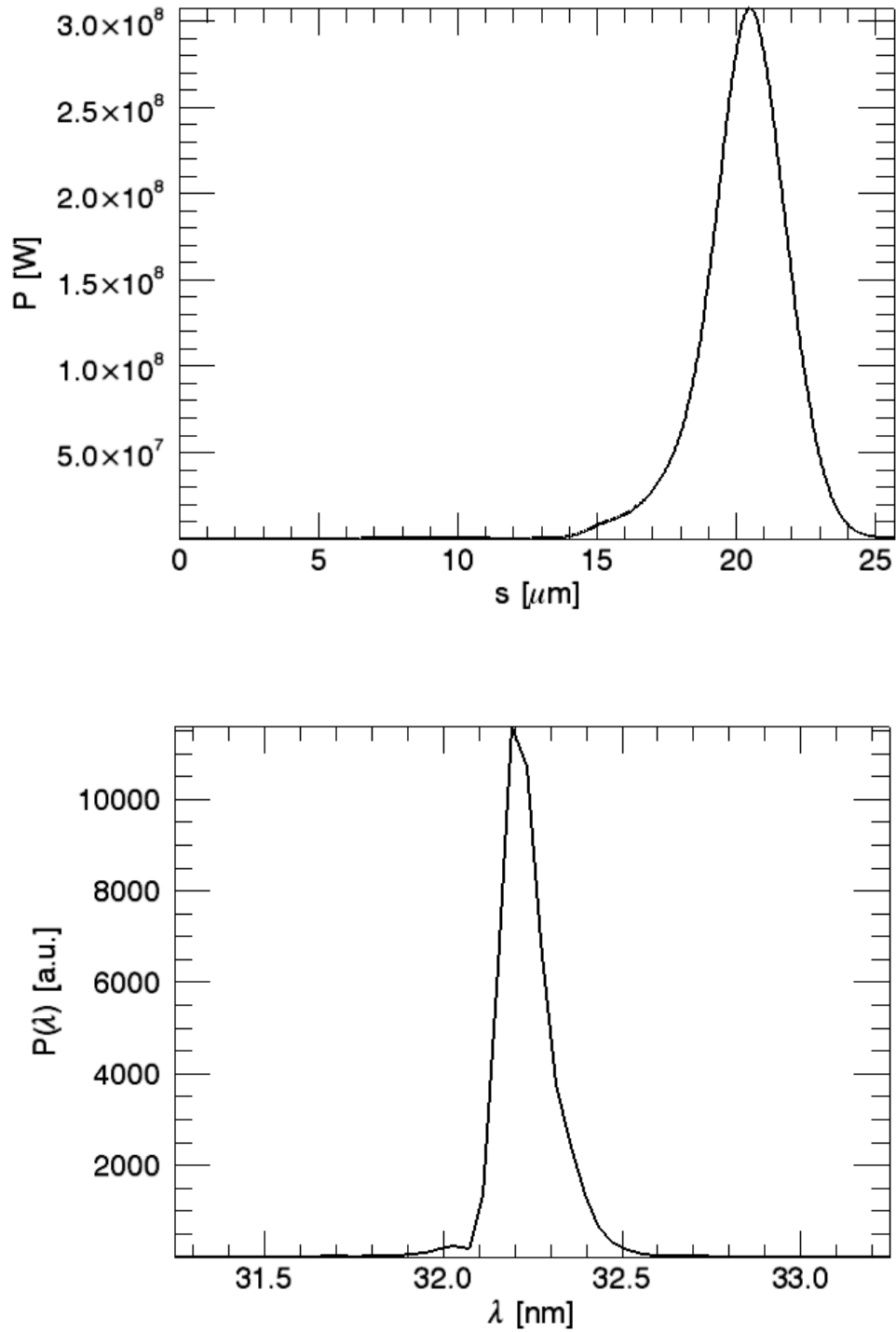


Figure 5.7: *Time resolved (top) and spectral (bottom) power distribution of the simulated FEL output for STARS with the helical-polarizing APPLE-III-type undulator tuned resonant to  $\lambda = 32.2$  nm and seeded with the low intensity HHG seed.*

### 5.3 HHG Seeding of the BESSY Low-Energy FEL

The final amplifier of the BESSY Low-Energy FEL was proposed to operate at wavelengths from  $10.33 \text{ nm}$  to  $51.0 \text{ nm}$  with an expected output power in the range of  $3.5 \text{ GW}$  -  $14 \text{ GW}$ . The electron beam is assumed to have an energy of  $1.02 \text{ GeV}$ , a peak current of  $1750 \text{ A}$ , a normalized emittance of  $1.5 \pi \text{ mm mrad}$  and a relative energy spread of  $2 \times 10^{-4}$ . The final amplifier will consist of two undulator modules. Each module has 69 periods with a period length of  $\lambda_u = 50 \text{ mm}$ . Inbetween the modules, drifts for quadrupoles and diagnostics are planned. In the present work, the final amplifier of the LE-FEL was tuned resonant to the 31st harmonic of the fundamental laser wavelength,  $\lambda_r = 23.9 \text{ nm}$ .

The seed for the LE-FEL case is depicted in figure 5.8. The FEL output for this HHG seed is shown in figure 5.9. Since the slippage length is significantly shorter for this case, a full separation of the seed and the FEL radiation can not occur inside the final amplifier. However, as a strong amplification of the desired wavelength will take place, the benefits of seeding with HHG radiation is still visible. The dominant effect is the enhanced purity of the spectrum compared to the HGHG configuration (see figures 3.10 and 3.11 in [19]).

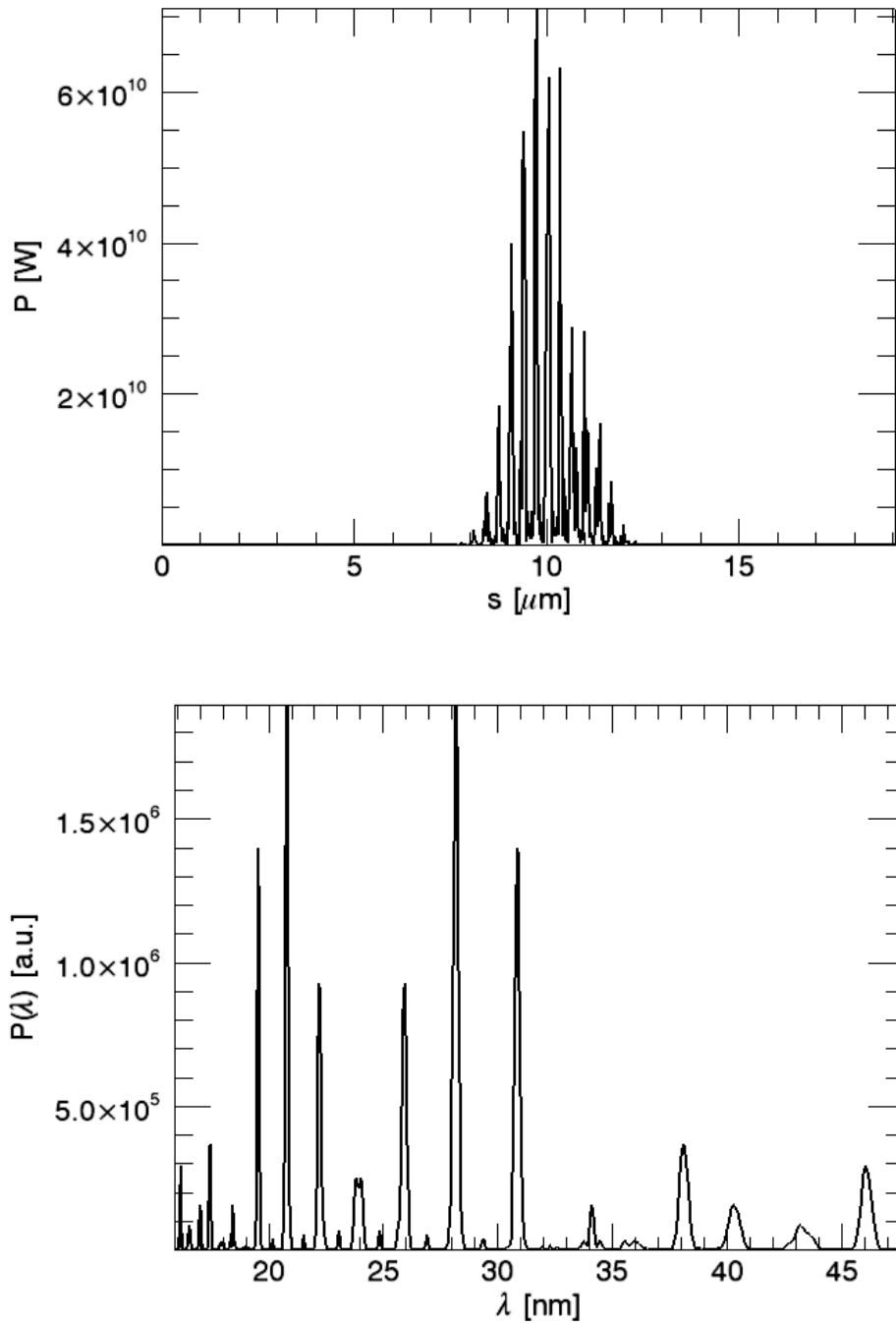


Figure 5.8: *Time resolved (top) and spectral (bottom) power distribution of the HHG seed, filtered and prepared for simulating the HHG seeded BESSY LE-FEL with GENESIS 1.3.*

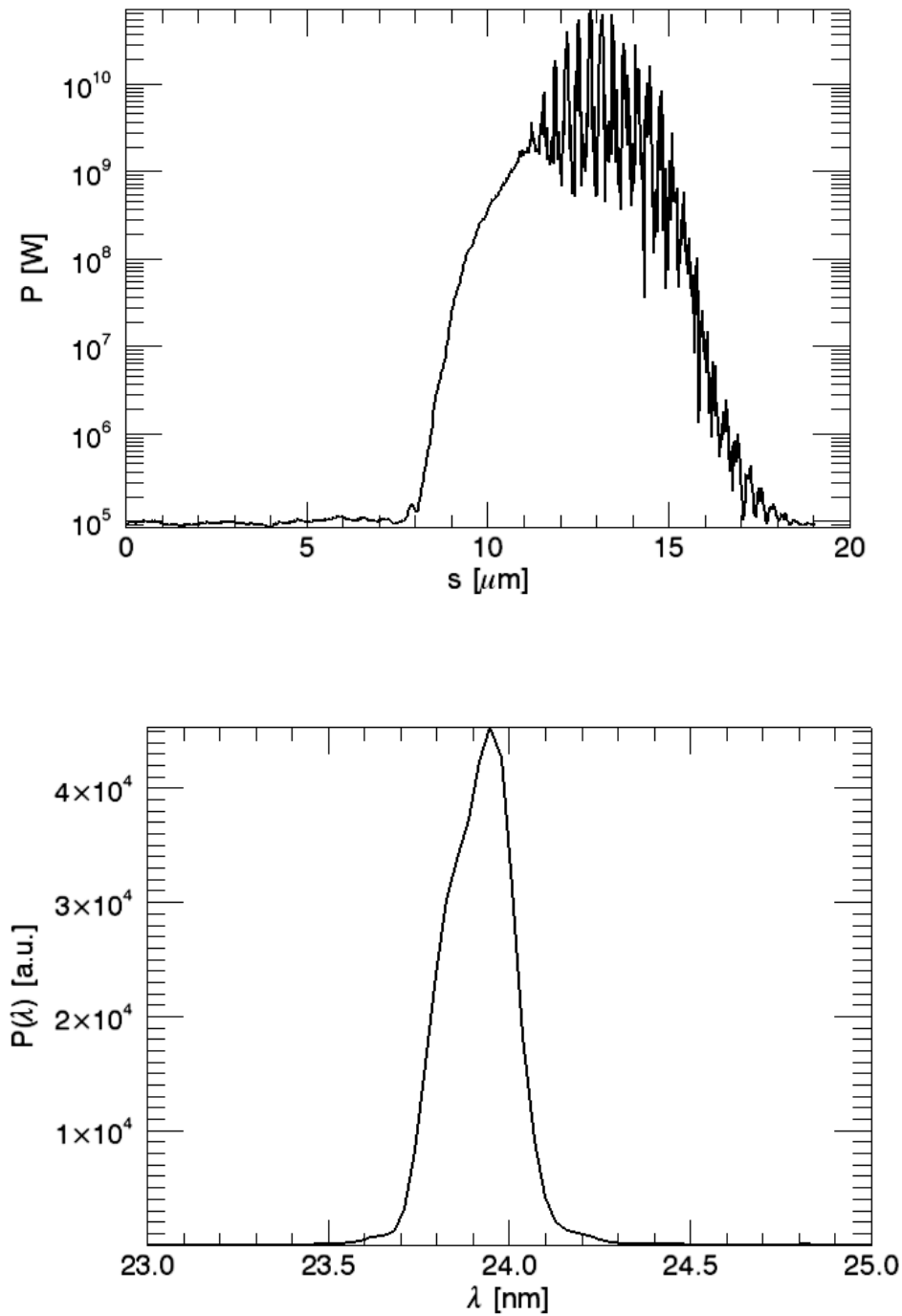


Figure 5.9: *Time resolved (top) and spectral (bottom) power distribution of the simulated FEL output for the HHG seeded BESSY LE-FEL tuned resonant to  $\lambda = 23.9$  nm. Since the seed and the FEL radiation are not fully separated, the time resolved distribution is depicted on a logarithmic scale to visualize the amplification of the radiation.*

---

## 6

# Conclusion

---

Due to the lack of suitable lasers, a variety of planned seeded FEL facilities, e.g. BESSY Soft X-ray FEL and STARS proposed by BESSY, will use the cascaded HHG scheme to provide high power seeds in the nanometer range. The High-order Harmonic Generation (HHG) process in gas medium offers the possibility to generate short wavelength seeds with needed high power. To allow for a numerical investigation of the new approach of HHG seeded FELs, a 3D simulation program for the HHG process in gases, based on the Strong-Field Approximation was developed. At first a semiclassical view on the HHG process, referred to as the Simple Man Model, was given in chapter 2. This model describes the basic features of the process in a concrete way. However, it is not sufficient to reproduce the HHG spectra. Therefore the Lewenstein Model was presented later on.

In chapter 3 the numerical implementation of the simulation code was described. This code calculates the dipole moment for a single atom induced in the HHG process and the formation of the macroscopic harmonic radiation. It takes into account the evolution of the fundamental laser beam and the generated XUV light through the gas medium. The program was written in  $C^{++}$  to allow for a portable application. The internal description of the electromagnetic fields is based on a fully radial symmetric geometry. The propagation of the fields is executed via a modified Crank-Nicholson differencing scheme. For this modified scheme a von Neumann stability analysis was performed to determine a stable set of grid parameters.

In chapter 4, results of HHG simulations were presented. It was shown that the code reproduces the main characteristics of HHG, i.e. phase-matching, the cut-off law and the behavior of the generated spectra under variation of the duration of the stimulating laser pulse. Hence, the validity of the underlying mathematical model could be proven. It was shown, that the simulation code is applicable to generate HHG spectra, which can be used to perform simulations of seeded FEL schemes.

Exemplarily, the final amplifiers of two HHG FELs, proposed to be built at BESSY, STARS and the low energy line of the BESSY-FEL, were simulated as HHG seeded FELs using the GENESIS 1.3 code. It was shown that replacing the HHG cascade by a HHG seed not only results in a shortened FEL setup, but also in a FEL output radiation of higher quality. The resulting spectra were cleaner, without sidebands as occurring in conventional HHG FELs.



---

# Appendix A

## Solution of the Schrödinger Equation

---

In section 2.2 the TDSE has to be solved within the Lewenstein Model, starting from the equation (2.20),

$$i|\dot{\Psi}\rangle = \hat{H}|\Psi\rangle , \quad (\text{A.1})$$

with the Hamiltonian

$$\hat{H} = -\frac{1}{2}\hat{\nabla}^2 + \hat{V}(\mathbf{r}) - E(t) \hat{x} \quad (\text{A.2})$$

and an Ansatz for the wave function, which neglects the depletion of the ground-state amplitude,

$$|\Psi\rangle = e^{iI_p t} \left( |0\rangle + \int d^3\mathbf{v} b(\mathbf{v}, t) |\mathbf{v}\rangle \right) , \quad (\text{A.3})$$

one can obtain the Schrödinger equation for the continuum state amplitudes  $b(\mathbf{v}, t)$  by multiplying eq.(A.1) with a test continuum state  $\langle \mathbf{w} |$  from the left side.

$$i\langle \mathbf{w} | \dot{\Psi} \rangle = \langle \mathbf{w} | \hat{H} | \Psi \rangle . \quad (\text{A.4})$$

With the time derivative of the wave function

$$i|\dot{\Psi}\rangle = -I_p|\Psi\rangle + ie^{iI_p t} \int d^3\mathbf{v} \dot{b}(\mathbf{v}, t) |\mathbf{v}\rangle ,$$

the left-hand-side of equation (A.4) reads as:

$$\begin{aligned} i\langle \mathbf{w} | \dot{\Psi} \rangle &= -I_p \langle \mathbf{w} | \Psi \rangle + ie^{iI_p t} \int d^3\mathbf{v} \dot{b}(\mathbf{v}, t) \langle \mathbf{w} | \mathbf{v} \rangle \\ &= -e^{iI_p t} I_p \langle \mathbf{w} | 0 \rangle + e^{iI_p t} \int d^3\mathbf{v} \left( -I_p b(\mathbf{v}, t) + i\dot{b}(\mathbf{v}, t) \right) \langle \mathbf{w} | \mathbf{v} \rangle \\ &= e^{iI_p t} \int d^3\mathbf{v} \left( -I_p b(\mathbf{v}, t) + i\dot{b}(\mathbf{v}, t) \right) \delta(\mathbf{w}, \mathbf{v}) \\ &= e^{iI_p t} \left( -I_p b(\mathbf{w}, t) + i\dot{b}(\mathbf{w}, t) \right) . \end{aligned} \quad (\text{A.5})$$

The right-hand-side  $\langle \mathbf{w} | \hat{H} | \Psi \rangle$  consists of three independent parts which should be discussed separately.

The first part represents the motion of a free electron:

$$\langle \mathbf{w} | -\frac{1}{2} \hat{\nabla}_{\mathbf{r}}^2 | \Psi \rangle = -\frac{1}{2} e^{iI_p t} \left\{ \langle \mathbf{w} | \hat{\nabla}_{\mathbf{r}}^2 | 0 \rangle + \int d^3\mathbf{v} b(\mathbf{v}, t) \langle \mathbf{w} | \hat{\nabla}_{\mathbf{r}}^2 | \mathbf{v} \rangle \right\}$$

$$\begin{aligned}
 &= -\frac{1}{2} e^{iI_p t} \int d^3\mathbf{v} b(\mathbf{v}, t) \langle \mathbf{w} | -\hat{\mathbf{v}}^2 | \mathbf{v} \rangle \\
 &= -\frac{1}{2} e^{iI_p t} \int d^3\mathbf{v} b(\mathbf{v}, t) \mathbf{v}^2 \langle \mathbf{w} | \mathbf{v} \rangle \\
 &= +\frac{1}{2} e^{iI_p t} \int d^3\mathbf{v} b(\mathbf{v}, t) \mathbf{v}^2 \delta(\mathbf{w}, \mathbf{v}) \\
 &= e^{iI_p t} \frac{\mathbf{w}^2 b(\mathbf{w}, t)}{2} \tag{A.6}
 \end{aligned}$$

The second term of the Hamiltonian represents the interaction of the electron and the atomic core potential  $V(\mathbf{r})$ . This term is negligible because when the electron appears in the continuum it is immediately accelerated by the intense laser field, at the outer point of the electron trajectory, the energy of the electron is relatively low, but also the potential nearly vanishes at far distances and lastly, when the electron returns to the nucleus, it has gained such a high momentum, that again the core attraction can be neglected.

Thus it follows:

$$\langle \mathbf{w} | \hat{V}(\mathbf{r}) | \Psi \rangle \approx 0 . \tag{A.7}$$

The laser and its interaction with the electron is determined by the last term of the Hamiltonian. To calculate its multiple with the test state, it is assumed that continuum to continuum (C-C) transitions do not contribute [4],

$$\langle \mathbf{w} | \hat{\mathbf{x}} | \mathbf{v} \rangle \approx -i \nabla_{\mathbf{v}} \delta(\mathbf{v} - \mathbf{w}) .$$

Further more, a basic identity for  $\delta$ -functions is used:

$$\int dx f(x) \frac{\partial}{\partial x} \delta(x - x_0) = - \left( \frac{\partial f}{\partial x} \right)_{x=x_0}$$

This leads to an expression for the laser-electron interaction part of the Hamiltonian,

$$\begin{aligned}
 \langle \mathbf{w} | -E(t) \hat{x} | \Psi \rangle &= -E(t) \langle \mathbf{w} | \hat{x} | \Psi \rangle \\
 &= -E(t) e^{iI_p t} \left\{ \langle \mathbf{w} | \hat{x} | 0 \rangle + \int d^3\mathbf{v} b(\mathbf{v}, t) \langle \mathbf{w} | \hat{x} | \mathbf{v} \rangle \right\} \\
 &= -E(t) e^{iI_p t} \left\{ d_x(\mathbf{w}) - i \int d^3\mathbf{v} b(\mathbf{v}, t) \frac{\partial}{\partial v_x} \delta(\mathbf{v} - \mathbf{w}) \right\} \\
 &= -E(t) e^{iI_p t} \left\{ d_x(\mathbf{w}) + i \left( \frac{\partial b(\mathbf{v}, t)}{\partial v_x} \right)_{\mathbf{v}=\mathbf{w}} \right\} . \tag{A.8a}
 \end{aligned}$$

In the above equation  $\mathbf{d}(\mathbf{v}) = \langle \mathbf{v} | \mathbf{x} | 0 \rangle$  denotes the atomic dipole matrix element for bound-free transitions;  $d_x(\mathbf{v})$  is the component parallel to the polarization axis of the laser.

---

Putting altogether leads to the time dependent Schrödinger equation for the amplitudes of the continuum states:

$$\dot{b}(\mathbf{v}, t) = -i \left( \frac{\mathbf{v}^2}{2} + I_p \right) b(\mathbf{v}, t) - E(t) \frac{\partial b(\mathbf{v}, t)}{\partial v_x} + iE(t) d_x(\mathbf{v}) \quad (\text{A.9})$$

The whole information about the atom is thus reduced to the form of  $\mathbf{d}(\mathbf{v})$ , and its complex conjugate  $\mathbf{d}^*(\mathbf{v})$  [4].

This differential Schrödinger type equation (A.9) can be solved exactly [4], leading to a closed form of  $b(\mathbf{v}, t)$ , using the laser  $E(t)$  and the corresponding vector potential  $\mathbf{A}(t) = \int_{-\infty}^t E(t') dt'$ .

$$b(\mathbf{v}, t) = i \int_0^t dt' E(t') d_x(\mathbf{v} + \mathbf{A}(t) - \mathbf{A}(t')) \times \exp \left\{ -i \int_{t'}^t dt'' [(\mathbf{v} + \mathbf{A}(t) - \mathbf{A}(t''))^2 / 2 + I_p] \right\} \quad (\text{A.10})$$

The expectation value of the position of the electron, which is equal to the induced dipole moment in atomic units, can be evaluated, so that the final equation for the dipole moment reads as:

$$x(t) = \langle \Psi(\vec{r}, t) | \hat{x} | \Psi(\vec{r}, t) \rangle = \int d^3\mathbf{v} d_x^*(\mathbf{v}) b(\mathbf{v}, t) + c.c. \quad (\text{A.11})$$

In a next step a change of variables to the canonical momentum  $\mathbf{p} = \mathbf{v} + \mathbf{A}(t)$  is performed as well as the quasiclassical action  $S(\mathbf{p}, t, t')$  is introduced. The quasiclassical action describes the motion of an electron moving freely in the laser electric field and therefore gives an additional phase factor  $\exp[-iS(\mathbf{p}, t, t')]$  to the dipole moment:

$$S(\mathbf{p}, t, t') = \int_{t'}^t dt'' \left( \frac{[\mathbf{p} - \mathbf{A}(t'')]^2}{2} + I_p \right). \quad (\text{A.12})$$

Note that with writing eq. (A.12), one also takes into account some effects of the binding atomic potential by introducing the ionization potential  $I_p$  into  $S(\mathbf{p}, t, t')$ , however as it is just an additional constant to the action, it neglects perturbations of the electronic wave function during the interaction with the laser.

Performing the change of variables and introducing  $S(\mathbf{p}, t, t')$ , the final expression for the dipole moment becomes:

$$x(t) = i \int_0^t dt' \int d^3\mathbf{p} d_x[\mathbf{p} - \mathbf{A}(t')] \times E(t')$$

$$\times d_x^* [\mathbf{p} - \mathbf{A}(t)] \times e^{-iS(\mathbf{p},t,t')} + c.c. \quad (\text{A.13})$$

The integral over the continuum states can be approximately solved via a stationary phase method, see appendix B, thus yielding the numerically computable expression for the laser induced atomic dipole moment as given in equation (2.30).

$$\begin{aligned} x(t) = & i \int_0^\infty d\tau \left( \frac{\pi}{\epsilon + i\tau/2} \right)^{3/2} \times E(t - \tau) \\ & \times d_x [p_{st}(t, \tau) - A_x(t - \tau)] \\ & \times d_x^* [p_{st}(t, \tau) - A_x(t)] \\ & \times \exp[-iS_{st}(t, \tau)] \\ & + c.c. \end{aligned} \quad (\text{A.14})$$

Here, the linearity of the laser was taken into account by writing  $A_x(t)$  instead of the whole vector potential  $\mathbf{A}(t)$ .

---

# Appendix B

## Stationary Phase Approximation

---

In mathematics, the stationary phase approximation is a basic principle of asymptotic analysis, applying to oscillatory integrals of the form

$$I(\lambda) = \int_a^b d^n x f(x) e^{i\lambda g(x)} \quad , \quad (\text{B.1})$$

where  $x \in R^n$  and  $f \in C$ ,  $g \in R$  are smooth enough to be approximated by a Taylor series near some point  $c \in [a, b]$ .

Suppose that  $g'(c) = 0$ , and that  $g'(x) \neq 0$  everywhere else in the considered interval and moreover that  $g''(c) \neq 0$  and  $f(c) \neq 0$ . Then the integral can be rewritten as

$$I(\lambda) = e^{i\lambda g(c)} \int_a^b d^n x f(x) e^{i\lambda [g(x) - g(c)]} \quad . \quad (\text{B.2})$$

The term  $e^{i\lambda [g(x) - g(c)]}$  is highly oscillatory for  $\lambda \gg 1$  and  $x \neq c$ , which causes the integral to decay very rapidly outside a small neighborhood around  $c$ . Thus, neglecting  $g(x)$ 's Taylor terms of the third and higher orders, one can approximate the integral:

$$\begin{aligned} I(\lambda) &\approx e^{i\lambda g(c)} \int_{c-\epsilon}^{c+\epsilon} d^n x f(x) e^{i\lambda [g(x) - g(c)]} \\ &\approx f(c) e^{i\lambda g(c)} \int_{c-\epsilon}^{c+\epsilon} d^n x e^{i\frac{\lambda}{2} g''(c) (x-c)^2} \\ &\approx f(c) e^{i\lambda g(c)} \int_{-\infty}^{+\infty} d^n x e^{i\frac{\lambda}{2} g''(c) (x-c)^2} \\ &= f(c) e^{i\lambda g(c)} \int_{-\infty}^{+\infty} d^n y e^{i\frac{\lambda}{2} g''(c) y^2} \quad . \end{aligned}$$

For a n-dimensional  $y \in R^n$ , the solution of the last integral is simply given by the complex gaussian integral, see for example [22]:

$$\begin{aligned} I(\lambda) &= f(c) e^{i\lambda g(c)} \prod_{j=1}^n \int_{-\infty}^{+\infty} dy_j e^{i\frac{\lambda}{2} g''(c) y_j^2} \\ &= f(c) e^{i\lambda g(c)} \left( \frac{2\pi i}{\lambda g''(c)} \right)^{n/2} \\ &= f(c) e^{i\lambda g(c)} \left( \frac{2\pi}{\lambda g''(c)} \right)^{n/2} e^{-in\pi/4} \quad . \end{aligned} \quad (\text{B.3})$$

In the derivation of the induced dipole moment in Lewenstein's Model an integral over all continuum states occurs, which can be solved via the stationary phase approximation.

In principle the dipole moment can be written as

$$x(t) = \int_0^\infty d\tau I(t, \tau) , \quad (\text{B.4})$$

with

$$I(t, \tau) = \int_{-\infty}^{+\infty} d^3p f(p, t, \tau) e^{-iS(p, t, \tau)} , \quad (\text{B.5})$$

as the integral to be approximated.

To perform the integration, a few preparations and definitions are helpful:

$$S_{st} := S(p_{st}, t, \tau) \quad (\text{B.6a})$$

$$S'_{st} := \frac{d}{dp} S(p, t, \tau)|_{p=p_{st}} := 0 \quad (\text{B.6b})$$

$$S''_{st} := \frac{d^2}{dp^2} S(p, t, \tau)|_{p=p_{st}} \quad (\text{B.6c})$$

$$f_{st} := f(p_{st}, t, \tau) \quad (\text{B.6d})$$

The quasi-classical action in  $I(t, \tau)$  is defined as:

$$\begin{aligned} S(p, t, \tau) &= \int_{t-\tau}^t dt' \left\{ \frac{(p - A(t'))^2}{2} + I_p \right\} \\ &= I_p \left\{ \tau + \frac{1}{2I_p} \int_{t-\tau}^t dt' (p - A(t'))^2 \right\} \end{aligned} \quad (\text{B.7})$$

In the last representation of (B.7) one can see that the form of  $S(p, t, \tau)$  corresponds to  $\lambda g(x)$  in the definition of the stationary phase approximation (B.1), thus the approximation is valid if  $I_p$  is comparably large. This is the case in the chosen regime of parameters because by definition HHG is a multi-photon process and  $I_p$  is as big as several photon energies.

In a next step, the stationary points of the action are derived via the condition  $\nabla_p S(p, t, \tau)|_{p=p_{st}} = 0$ , given in (B.6b):

$$\begin{aligned} 0 &\stackrel{!}{=} \frac{d}{dp} S(p, t, \tau)|_{p=p_{st}} = \int_{t-\tau}^t dt' ((p_{st} - A(t'))) = p_{st}\tau - \int_{t-\tau}^t dt' A(t') \\ &\implies p_{st}(t, \tau) = \frac{1}{\tau} \int_{t-\tau}^t dt' A(t') \end{aligned} \quad (\text{B.8})$$

---


$$\implies S_{st}(t, \tau) = (I_p - \frac{1}{2} p_{st}^2) \tau + \frac{1}{2} \int_{t-\tau}^t dt' A^2(t') \quad (\text{B.9})$$

This means that the stationary momentum corresponds to the average vector potential an electron has seen during its flight. Furthermore the definition of the action in classical mechanics  $S = \int_{p_1}^{p_2} p dx$  implies,

$$\nabla_p S(p, t, \tau) = x(t) - x(t - \tau) , \quad (\text{B.10})$$

which illustrates, that the stationary points of the quasi-classical action are those momenta  $p$  for which an electron born at time  $t - \tau$  returns to the same position at time  $t$ . As a matter of fact  $x(t)$  and  $x(t - \tau)$  have to be close to the origin at the nucleus because it is the only position where a transition from or to the groundstate is possible.

In order to accomplish the calculation of the considered integral one also needs to know the second derivative of  $S(p, t, \tau)$  at it's stationary points, in fact it turns out that  $\frac{d^2}{dp^2} S(p, t, \tau)$  is constant for any momentum  $p$ :

$$\begin{aligned} S''(p, t, \tau) &= \frac{d^2}{dp^2} S(p, t, \tau) \\ &= \frac{d^2}{dp^2} \int_0^\tau dt' \left\{ \frac{(p - A(t'))^2}{2} + I_p \right\} \\ &= \frac{d}{dp} \int_0^\tau dt' \{(p - A(t'))\} \\ &= \int_0^\tau dt' = \tau . \end{aligned}$$

$$\implies S''_{st} = \tau . \quad (\text{B.11})$$

With these preparations, the quasi-classical action can be expanded as a Taylor series around the stationary momentum  $p_{st}$ :

$$S(p, t, \tau) = S_{st} + \frac{1}{2} S''_{st} (p - p_{st})^2 + O(p^3) . \quad (\text{B.12})$$

Then the integral in equation (B.5) can be calculated by using the complex gaussian integration method,

$$\begin{aligned} I(t, \tau) &= e^{-iS_{st}} \int_{-\infty}^{+\infty} d^3p f(p, t, \tau) e^{-i[S(p, t, \tau) - S_{st}]} \\ &\approx e^{-iS_{st}} \int_{-\infty}^{+\infty} d^3p f(p, t, \tau) e^{-\frac{i}{2} S''_{st} (p - p_{st})^2} \\ &\approx e^{-iS_{st}} f_{st} \int_{-\infty}^{+\infty} d^3y e^{-i\frac{\tau}{2} y^2} \end{aligned}$$

$$= e^{-iS_{st}} f_{st} \left( \frac{\pi}{i\tau/2} \right)^{3/2} . \quad (\text{B.13})$$

Thus the dipole moment takes the form:

$$x(t) = \int_0^\infty d\tau I(t, \tau) = \int_0^\infty d\tau \left( \frac{\pi}{i\tau/2} \right)^{3/2} f_{st}(t, \tau) e^{-iS_{st}(t, \tau)} . \quad (\text{B.14})$$

Evaluating the last integral requires the introduction of a infinitely small imaginary regularization constant to avoid the singularity at  $\tau = 0$  inside. This is done by a substitution  $\tau \rightarrow \tau - 2i\epsilon$  inside the prefactor, thus yielding an approximate result for the induced dipole moment of Lewenstein's Model as introduced in section 2.2, equation (2.30):

$$x(t) = \int_0^\infty d\tau \left( \frac{\pi}{\epsilon + i\tau/2} \right)^{3/2} f(p_{st}, t, \tau) e^{-iS(p_{st}, t, \tau)} . \quad (\text{B.15})$$

The validity of the introduction of such a regularization constant could be proven by varying  $\epsilon$  over the range of several orders of magnitude (  $10^{-32}$  upto  $10^{-3}$  ) without affecting the numerical result of the integral.

---

# Appendix C

## Stability Analysis of the Propagation Routine

---

A very important property of a differencing scheme is its stability. In textbooks, e.g. [18], unconditional stability is proposed for the CN scheme. Unfortunately, this is not completely true for a radial symmetric grid due to the  $(1/r)$ -term in the Laplacian, see eq.(3.19). To study the stability of the differencing scheme given in eq.(3.20), a *von Neumann stability analysis* was performed. The von Neumann analysis is a local method, where the coefficients of the differencing equations are considered as constant in  $r$ - and  $z$ -space. In that case the independent solutions of the underlying partial differential equation under neglect of the source term can be written in terms of transverse eigenmodes of the form

$$v_j^n(k) = \xi^n(k) e^{ikj\Delta r} , \quad (\text{C.1})$$

for any real wavenumber  $k$  in the transverse direction and with  $\xi^n(k)$  denoting the amplitude of the corresponding eigenmode after the  $n$ -th iteration step. In a next step, these eigenmodes are supplied to the differencing scheme, which is then solved for the amplification factor

$$g(k) = \frac{\xi^{n+1}}{\xi^n} . \quad (\text{C.2})$$

The differencing scheme is stable for those eigemodes  $v_j^n(k)$ , where

$$|g(k)|^2 \leq 1 . \quad (\text{C.3})$$

The underlying differencing scheme, referring to eq.(3.20), reads as

$$v_j^{n+1} - v_j^n = -i\alpha [\gamma_j^+(v_{j+1}^{n+1} + v_{j+1}^n) + \gamma_j^-(v_{j-1}^{n+1} + v_{j-1}^n) - 2(v_j^{n+1} + v_j^n)] , \quad (\text{C.4})$$

with

$$\gamma_j^\pm = 1 \pm \frac{1}{2j} > 0, \in \mathbb{R} \quad \alpha = \frac{c\Delta z}{\omega(\Delta r)^2} > 0, \in \mathbb{R} . \quad (\text{C.5})$$

Applying the eigenmodes to the differencing scheme, eq.(C.4), results in:

$$(g - 1)v_j^n = -i\alpha [\gamma_j^+ e^{+ik\Delta r} + \gamma_j^- e^{-ik\Delta r} - 2] (g + 1)v_j^n . \quad (\text{C.6})$$


---

Solving for  $g$  yields:

$$\begin{aligned}
 g &= \frac{1 - i\alpha [\gamma_j^+ e^{+ik\Delta r} + \gamma_j^- e^{-ik\Delta r} - 2]}{1 + i\alpha [\gamma_j^+ e^{+ik\Delta r} + \gamma_j^- e^{-ik\Delta r} - 2]} \\
 &= \frac{1 - i\alpha [(\gamma_j^+ + \gamma_j^-) \cos(k\Delta r) + i(\gamma_j^+ - \gamma_j^-) \sin(k\Delta r) - 2]}{1 + i\alpha [\dots]} \\
 &= \frac{1 + \frac{\alpha}{j} \sin(k\Delta r) - 2i\alpha [\cos(k\Delta r) - 1]}{1 - \frac{\alpha}{j} \sin(k\Delta r) + 2i\alpha [\cos(k\Delta r) - 1]} . \tag{C.7}
 \end{aligned}$$

Thus stability is given if:

$$|g|^2 = \frac{(1 + \frac{\alpha}{j} \sin(k\Delta r))^2 + 4(\alpha [\cos(k\Delta r) - 1])^2}{(1 - \frac{\alpha}{j} \sin(k\Delta r))^2 + 4(\alpha [\cos(k\Delta r) - 1])^2} \leq 1$$

$$\implies (1 + \frac{\alpha}{j} \sin(k\Delta r))^2 \leq (1 - \frac{\alpha}{j} \sin(k\Delta r))^2$$

$$2\frac{\alpha}{j} \sin(k\Delta r) \leq -2\frac{\alpha}{j} \sin(k\Delta r)$$

$$\alpha \sin(k\Delta r) \leq -\alpha \sin(k\Delta r) . \tag{C.8}$$

Hence one has to distinguish between two cases,  $\alpha < 0$  and  $\alpha > 0$ . For the first case the final condition reads as:

$$\sin(k\Delta r) \geq 0 ,$$

$$\implies 2n\pi \leq k\Delta r \leq (2n + 1)\pi , n \in \mathbb{Z} . \tag{C.9}$$

As  $\alpha$  was restricted to be greater than 0 in the present work, the stability criterion of interest is given by:

$$\sin(k\Delta r) \leq 0 ,$$

$$\implies (2n - 1)\pi \leq k\Delta r \leq 2n\pi , n \in \mathbb{Z} . \tag{C.10}$$

---

# Appendix D

## Additional HHG Spectra

---

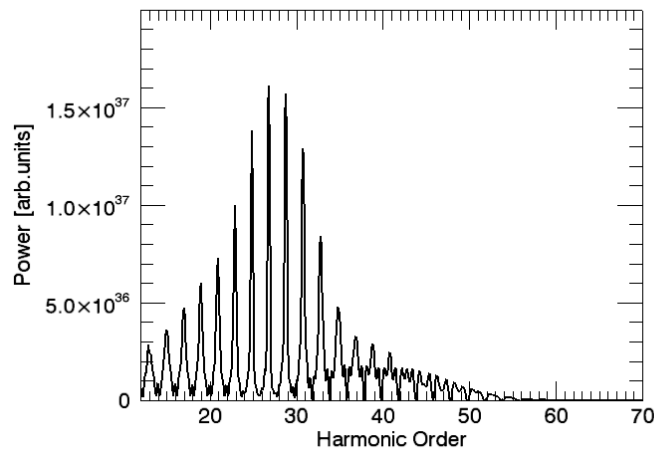
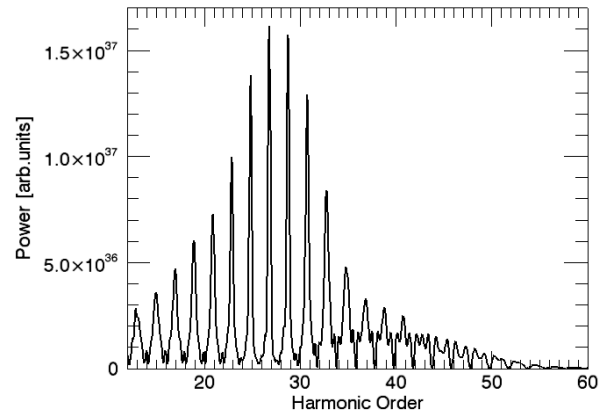
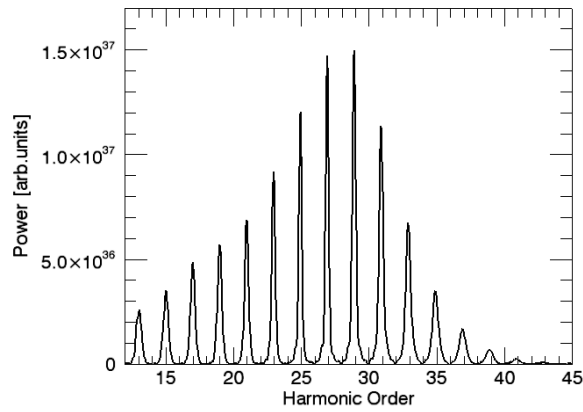


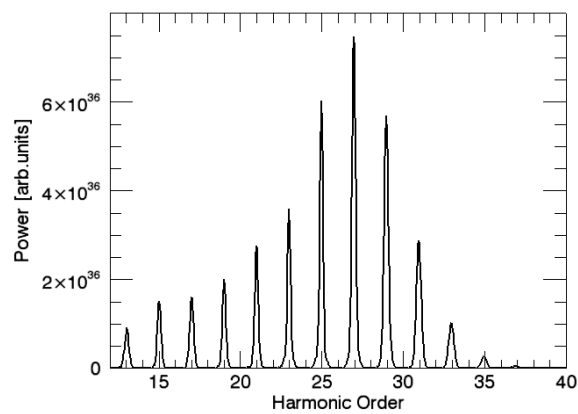
Figure D.1: *HHG power spectrum for a constant peak intensity of the fundamental laser  $I_0 = 7.5 * 10^{14} \text{ W/cm}^2$  and a pulse duration of  $\tau = 10 \text{ fs}$ , resulting in a total pulse energy of  $E = 0.61 \text{ mJ}$*



$$\tau = 10 \text{ fs}, I_0 = 7 * 10^{14} \text{ W/cm}^2$$



$$\tau = 15 \text{ fs}, I_0 = 4.67 * 10^{14} \text{ W/cm}^2$$



$$\tau = 20 \text{ fs}, I_0 = 3.5 * 10^{14} \text{ W/cm}^2$$

Figure D.2: *HHG power spectra for different pulse durations and peak intensities with a constant total pulse energy of the fundamental laser  $E = 0.57 \text{ mJ}$ .*

---

# Bibliography

---

- [1] D. Krämer, E. Jaeschke, and W. Eberhardt, editors. *The BESSY Soft X-ray Free Electron Laser, Technical Design Report*. BESSY GmbH Berlin Adlershof, 2004.
- [2] L. H. Yu and J. Wu. Theory of high gain harmonic generation: an analytical estimate. *Nuclear Instruments and Methods in Physics Research Section A*, 483:493–498, 2002.
- [3] E.L. Saldin, E.A. Schneidmiller, and M.V. Yurkov. Study of a noise degradation of amplification process in a multistage HGHG FEL. *Opt. Commun.*, 202:169, 2002.
- [4] M. Lewenstein, Ph. Balcou, M. Yu. Ivanov, A. L’Huillier, and P. B. Corkum. Theory of high-harmonic generation by low-frequency laser fields. *Phys. Rev. A*, 49(3):2117, 1994.
- [5] S. Reiche. Numerical studies for a single-pass high gain free-electron laser. *PhD-thesis Universität Hamburg and Nuclear Instruments and Methods in Physics Research A*, 429:243, 1999.
- [6] *Visions of Science: The BESSY SASE-FEL in Berlin Adlershof*. BESSY GmbH Berlin Adlershof, <http://www.bessy.de/fel>, 2001.
- [7] B.W.J. McNeil, N.R. Thompson, and B. Sheehy. The conceptual design of the 4GLS XUV-FEL. In *Proceedings of the 28th Free Electron Laser Conference*, Berlin, 2006.
- [8] G. De Ninno, E. Allaria, W. Fawley, and G. Penn. Design and performance of the FERMI at ELETTRA FEL. In *Proceedings of the 28th Free Electron Laser Conference*, Berlin, 2006.
- [9] L. Giannessi et al. Future seeding experiments at SPARC. In *Proceedings of the 28th Free Electron Laser Conference*, Berlin, 2006.
- [10] M. Altarelli, R. Brinkmann, M. Chergui, W. Decking, B. Dobson, S. Düsterer, G. Grübel, W. Graeff, H. Graafsma, J. Hajdu, J. Marangos, J. Pflüger, H. Redlin, D. Riley, I. Robinson, J. Rossbach, A. Schwarz, K. Tiedtke, T. Tschentscher, I. Vartaniants, H. Wabnitz, H. Weise, R. Wichmann, K. Witte, A. Wolf, M. Wulff, and M. Yurkov, editors. *X-FEL - The European X-Ray Free Electron Laser, Technical Design Report*. DESY XFEL Project Group and European XFEL Project Team and Deutsches Elektronen-Synchrotron Member of the Helmholtz Association, 2006.

- [11] E.L. Saldin, E.A. Schneidmiller, and M.V. Yurkov. *The Physics of Free Electron Lasers*. Springer-Verlag Berlin Heidelberg, 2000.
- [12] B. W. J. McNeil, J. A. Clarke, D. J. Dunning, G. J. Hirst, H. L. Owen, N. R. Thompson, B. Sheehy, and P. H. Williams. An XUV-FEL amplifier seeded using high harmonic generation. *New Journal of Physics*, 9(4):82, 2007.
- [13] B. W.J. McNeil, D. J. Dunning, N. Thompson, and B. Sheehy. The use of HHG at 4GLS. In *Proceedings of the 28th Free Electron Laser Conference*, Berlin, 2006.
- [14] L. Giannessi, M. Quattromini, P. Musumeci, M. Nisoli, G. Sansone, S. Stagira, and S. de Silvestri. Analysis of the process of amplification in a single pass FEL of high order harmonics generated in a gas jet. In *Proceedings of the 28th Free Electron Laser Conference*, Berlin, 2006.
- [15] C. Rullière, editor. *Femtosecond Laser Pulses*. Springer Berlin, 2nd edition, 2005.
- [16] M. Ammosov, M. Delone, and V. Kraїnov. Tunnel ionization of complex atoms and atomic ions in an alternating electromagnetic field. *Sov.Phys JETP*, 64:1191, 1986.
- [17] E. Priori, G. Cerullo, M. Nisoli, S. Stagira, S. De Silvestri, P. Villoresi, L. Poletto, P. Ceccherini, C. Altucci, R. Bruzzese, and C. de Lisio. Nonadiabatic three-dimensional model of high-order harmonic generation in the few-optical-cycle regime. *Phys. Rev. A*, 61(6):063801, 2000.
- [18] W.H. Press, B.P. Flannery, S.A. Teukolsky, and W.T. Vetterling. *Numerical Recipes in C: The Art of Scientific Computing*. Cambridge University Press, 2nd edition, 1992.
- [19] T. Kamps et al. STARS - A two-stage high-gain harmonic generation FEL demonstrator. In *Proceedings of the 22nd Particle Accelerator Conference*, Albuquerque, New Mexico, USA, 2007.
- [20] J. G. Eden. High-order harmonic generation and other intense optical field-matter interactions: review of recent experimental and theoretical advances. *Progress in Quantum Electronics*, 28(3-4):197–246, 2004.
- [21] Kathrin Goldammer. *Studies of Harmonic Generation in Free Electron Lasers*. PhD thesis, Humboldt-Universität zu Berlin, 2007.
- [22] M. Nakahara. *Geometry, Topology and Physics*. Kinki University, Osaka, Japan, 2nd edition, 2003.

---

# Acknowledgment

---

First of all I would like to thank Prof. Eberhard Jaeschke for giving me the opportunity to write my diploma thesis at BESSY and examining it.

I thank Dr. Alejandro Saenz for serving as a second consultant of this thesis.

I also thank Dr. Atoosa Meseck, who stimulated my interest in the field of High-order Harmonic Generation and its usability for seeded FELs. I give props to her for the patience she always had with me and all the thousands of questions I had, the pleasant working atmosphere and her enthusiasm which always motivated me during this year.

I would like to thank Dr. Jérôme Gaudin for taking time to demonstrate a real HHG experiment to me and Dr. Philippe Wernet for a fruitful discussion.

I would like to thank the colleagues of BESSY, first of all Dr. Johannes Bahrtdt for giving me my first student job at BESSY and Kathrin Goldammer for first citing me, Torsten Quast and Rolf Mitzner for helpful tips and all the other BESSY members for the friendly working environment.

I would also like to thank the colleagues of the Max-Planck Institute for Quantum Optics in Garching, especially Dr. Vladislav S. Yakovlev for his very precise and helpful summary on HHG.

I thank Nils Krebs, Simon Hauser and Silke Schwarz for reading the thesis and Andreas Rodigast for good L<sup>A</sup>T<sub>E</sub>X tips and discussions on some mathematical issues.

A very special thank goes to Jessica for always having been there for me.

Above all I thank my parents for their unconditional support at all times and for their encouragement.

# Erklärung

Hiermit erkläre ich, dass ich die Diplomarbeit selbstständig verfasst und keine anderen als die angegebenen Quellen und Hilfsmittel verwendet habe.  
Ich bin mit der Auslage meiner Diplomarbeit in den Bibliotheken der Humboldt-Universität zu Berlin einverstanden.

Berlin, den 13. August 2007

Torsten Leitner